Journal of Glaciology

Article

Cite this article: Partington G, Copland L, Lauzon B, Medrzycka D, Main B, Kochtitzky WH, Dow CF (2025) Surge history and dynamics of Fisher Glacier, Yukon, 1948–2022. *Journal of Glaciology* **71**, e100, 1–19. https://doi.org/10.1017/jog.2025.10084

Received: 18 March 2025
Revised: 21 August 2025
Accepted: 21 August 2025

Keywords:
glacier fluctuations; glacier surges; ice velocity

Corresponding author: Luke Copland;
Email: luke.copland@uottawa.ca

Surge history and dynamics of Fisher Glacier, Yukon, 1948–2022

Gabriel Partington[1], Luke Copland[1], Benoît Lauzon[1], Dorota Medrzycka[1], Brittany Main[1,2], William Hardy Kochtitzky[3] and Christine F. Dow[2]

[1]Department of Geography, Environment and Geomatics, University of Ottawa, Ottawa, ON, Canada; [2]Department of Geography and Environmental Management, University of Waterloo, Waterloo, ON, Canada and [3]School of Marine and Environmental Programs, University of New England, Biddeford, ME, USA

Abstract

Remotely sensed datasets indicate that Fisher Glacier underwent two surges since 1948: during approximately 1969–72 and 2013–16. These were characterized by an advanced terminus position (terminus-wide average advance 571 ± 143 m from 1963 to 1972 and 868 ± 8 m from 2014 to 2017), intense surface crevassing (up to >30 km up-glacier from the terminus during both surges), high surface velocities and a down-glacier transfer of mass. The intervening quiescent phase lasted for 40 years, during which velocities were generally low (<50 m a^{-1}), but underwent a slow multidecadal increase starting around 1985, spreading from the middle of the glacier. A pre-surge buildup phase beginning around 2008 resulted in velocities of up to ~200 m a^{-1}. The active phase of the surge initiated in winter 2013/14, with velocities of up to 1500 m a^{-1} propagating both up- and down-glacier from the mid-glacier region. In July 2016, the surge rapidly terminated within a period of ~1 month. Characterized by a rapid onset and termination, but also displaying a multidecadal acceleration prior to the surge, the cause of Fisher Glacier's surges may be best explained by a unifying framework such as the enthalpy balance theory.

1. Introduction

Surge-type glaciers are characterized by dynamic instabilities that result in periodic alternating cycles of fast flow, termed the active phase, and slow flow, termed the quiescent phase (Meier and Post, 1969; Sevestre and Benn, 2015). Active phase velocities are usually at least an order of magnitude higher than quiescent flow speeds (Meier and Post, 1969), and quiescent phase velocities are almost always slower than velocities on neighboring non-surge-type glaciers (Burgess and others, 2013). The documentation of repeat surge events, particularly in Yukon/Alaska (Eisen and others, 2001, 2005; Bevington and Copland, 2014; Abe and others, 2016; Kochtitzky and others, 2019; Nolan and others, 2021) and Svalbard (Sund and others, 2009; Sevestre and others, 2015), indicates that the active phase generally lasts for <1 to ~5 years for a temperate glacier, and ~2 to 20 years for a polythermal glacier.

The traditional consensus is that two main mechanisms drive glacier surges: changes in basal thermal conditions on polythermal glaciers, and changes in basal hydrological conditions on temperate glaciers (Kamb and others, 1985; Murray and others, 2003). While some regions such as Yukon/Alaska tend to be heavily influenced by hydrological controls, and surges in areas like Svalbard and the Canadian High Arctic tend to be influenced by thermal controls (Jiskoot and others, 2000), there are numerous cases where these mechanisms do not explain a glacier's surging behavior (Herreid and Truffer, 2016; Benn and others, 2022). More recently, the enthalpy balance theory has been proposed as a way of explaining glacier surging based on changes in energy content of a glacier, regardless of the exact mechanisms at play (Sevestre and Benn, 2015; Benn and others, 2019a, 2019b, 2022). According to this theory, climate seems to be a first-order, global control on the distribution of surge clusters, whereas glacier geometry is a second-order, regional control.

The mountain ranges of Yukon/Alaska are home to one of the world's largest clusters of surge-type glaciers. Meier and Post (1969) identified 204 glaciers there as being surge-type, and in the St. Elias Mountains specifically, 151 glaciers were classified as surge-type by Clarke and others (1986). With access to better data, the number of surge-type glaciers in the St. Elias Mountains was updated to 46 observed, 93 probable and 105 possible in the Randolph Glacier Inventory v7 (RGI Consortium, 2023). Studies over the past decade have provided increasingly detailed information about the surges of major glaciers on the eastern side of the St. Elias Mountains, such as Nàłùdäy (Lowell Glacier) (Bevington and Copland, 2014), Dän Zhùr (Donjek Glacier)

(Abe and others, 2016; Kochtitzky and others, 2019), Little Kluane (Main and others, 2024), Klutlan (Altena and others, 2019), Dusty (Young and others, 2024) and Tweedsmuir (Sharp, 2021). However, to date there has been no detailed study of the surge characteristics of Fisher Glacier, the largest remaining surge-type glacier in this region without such an analysis. Documenting the diversity of surge behaviors is critical to better understanding the mechanisms driving the spectrum of dynamic instabilities that are observed on glaciers globally.

The objectives of this study are to reconstruct the surge history of Fisher Glacier by measuring the frequency, duration and location of past surges, and to assess the primary factors that control its surging. This is undertaken using a variety of remote sensing datasets and field observations from the past ~75 years, including air photos, satellite images, digital elevation models (DEMs) and surface velocities.

2. Study area

The St. Elias Mountains, which form the largest non-polar icefield in the world, contain a glacierized area of ~32,900 km^2, with glacier elevations varying between 0 and 5930 m above sea level (a.s.l.). Both surge-type and non-surge-type glaciers in Yukon/Alaska have been losing mass recently, with a regional mass trend of −72.5 ± 8 Gt a^{-1} from 2002 to 2019 (Ciracì and others, 2020). Annual air surface temperatures in the St. Elias Mountains have been increasing since 1979 at all elevations from 2000 to 6000 m a.s.l., with a maximal rate 1.6× larger than the global-mean rate (0.028°C a^{-1} vs. 0.017°C a^{-1}) at the highest elevations (5500–6000 m a.s.l.) from 1970 to 2015 (Williamson and others, 2020).

Fisher Glacier is a large valley glacier located in Kluane National Park in the southeastern portion of the St. Elias Mountains (60°04′56″ N, 138°03′46″ W), is ~45 km long, an average of 3.8 km wide, and covers an area of >400 km^2 (Fig. 1). Its terminus is located around 500 m a.s.l., and it drains eastward into the Alsek River, which flows mainly south into the Gulf of Alaska. The top of the main accumulation zone extends to an elevation of >1500 m, shared with Nàłùdäy, which flows parallel to Fisher Glacier ~20 km to the north. A weather station located on a nunatak at 1248 m a.s.l. on Nàłùdäy (Fig. 1b), near the equilibrium line, recorded a mean annual air temperature of −4.1°C over 2019–23.

Previous studies on Fisher Glacier are limited. One of the earliest mentions of the glacier is by Clarke and Holdsworth (2002, p. J312), who state that 'Fisher Glacier […] surged around 1970, but little information about this event is available', but provide no further details. Burgess and others (2013) provide a velocity map which shows winter velocities of around 0.1–0.3 m d^{-1} (37–110 m a^{-1}) from 2007 to 2011, while Van Wychen and others (2018) show similar winter velocities of ~40 m a^{-1} in 2007–08 and ~60 m a^{-1} in 2009–10. More recently, Altena and others (2019) mentioned that an increase in speed was observed on Fisher Glacier from 2013 to 2018, reaching velocities of about 4 m d^{-1} (1460 m a^{-1}).

3. Methods

3.1. Changes in terminus extent

Terminus extents were quantified for the period 1948–2022 from a total of 66 air photos and satellite images (Supplementary Table S1), including sub-annual changes between August 2013 and August 2017 during a period of rapid terminus advance. The up-glacier boundary of these terminus extents was clipped to a common line in the ablation zone, located ~3.4 km up-glacier from the maximum terminus extent, past which the terminus never retreated (Fig. 2). Terminus changes were measured using the Glacier Termini Tracking (GTT) toolbox in ArcGIS Pro (Urbanski, 2018). The GTT toolbox uses digitized terminus extents to determine two-dimensional rates of change by measuring the distance between points at user-designated intervals along terminus outlines with different dates (Urbanski, 2018). This was undertaken once for the entire length of the terminus at a point interval of 100 m to provide a measure of total mean retreat, and then once for each of three subsections titled the Northern Terminus, Central Terminus and Southern Terminus (Fig. 2), at a point interval of 50 m.

For the pre-satellite era (before 1972), historical air photos, taken by the Royal Canadian Air Force (RCAF), were acquired from the National Air Photo Library in Ottawa, Ontario and the Yukon Energy, Mines and Resources Library in Whitehorse, Yukon (Supplementary Table S1). The 1948, 1954, 1972 and 1976 termini were mapped from orthorectified images generated from nadir air photos taken by the RCAF from an altitude ranging between 10,500 and 40,000 ft (3200 to 12,192 m), depending on year, and typically scanned at 600 dots per inch (see procedure outlined in 3.4.1).

For the satellite era, at least one summer (May–September) cloud-free optical satellite image was acquired for each year from 1973 to 2022 (Supplementary Table S1). Images from July to September were prioritized when available to ensure consistent temporal separation and minimal snow cover. Terminus outlines from 1963 and 1977 were delineated from two declassified satellite images from the KH-5 Argon and KH-9 Hexagon projects, respectively, obtained from the United States Geological Survey (USGS) EarthExplorer (https://earthexplorer.usgs.gov/). Both declassified satellite images were manually georeferenced to a 3 m resolution PlanetScope image from 4 July 2022 using affine transformation, with nine ground control points (GCPs) for 1963, and eight for 1977. The RCAF orthomosaics were manually georeferenced to the same PlanetScope image.

Landsat 1–4 Multispectral Scanner (MSS) images and Landsat 5 Thematic Mapper (TM) images were obtained from USGS EarthExplorer for the period 1973–87, for the most part as precision and terrain corrected files, which means that no further georeferencing or pre-processing was required. Historical SPOT 1–3 imagery from 1988 to 1996 were downloaded from the USGS EarthExplorer, while SPOT 4–5 images from 2001 to 2009 were downloaded from CNES's Spot World Heritage Programme (https://regards.cnes.fr/user/swh/modules/60). Most of the SPOT images were downloaded as L1A products and required slight geometrical corrections of up to a few pixels, using the Shift function in ArcGIS Pro to align the terminus area with a recent PlanetScope or RapidEye image. Landsat 5 TM and 7 Enhanced Thematic Mapper Plus (ETM+) images (downloaded from USGS EarthExplorer), and one Advanced Spaceborne Thermal Emission and Reflection Radiometer (ASTER) scene (downloaded from NASA Earthdata; https://www.earthdata.nasa.gov/), were used to fill gaps when no SPOT or other higher resolution images were available. RapidEye 1–4 and PlanetScope images were acquired courtesy of Planet Images, through their Education and Research Program, and covered the period 2010–22.

Uncertainties associated with the terminus change rates are dependent on the georeferencing error for images that were manually corrected, and on the ground resolution of the imagery.

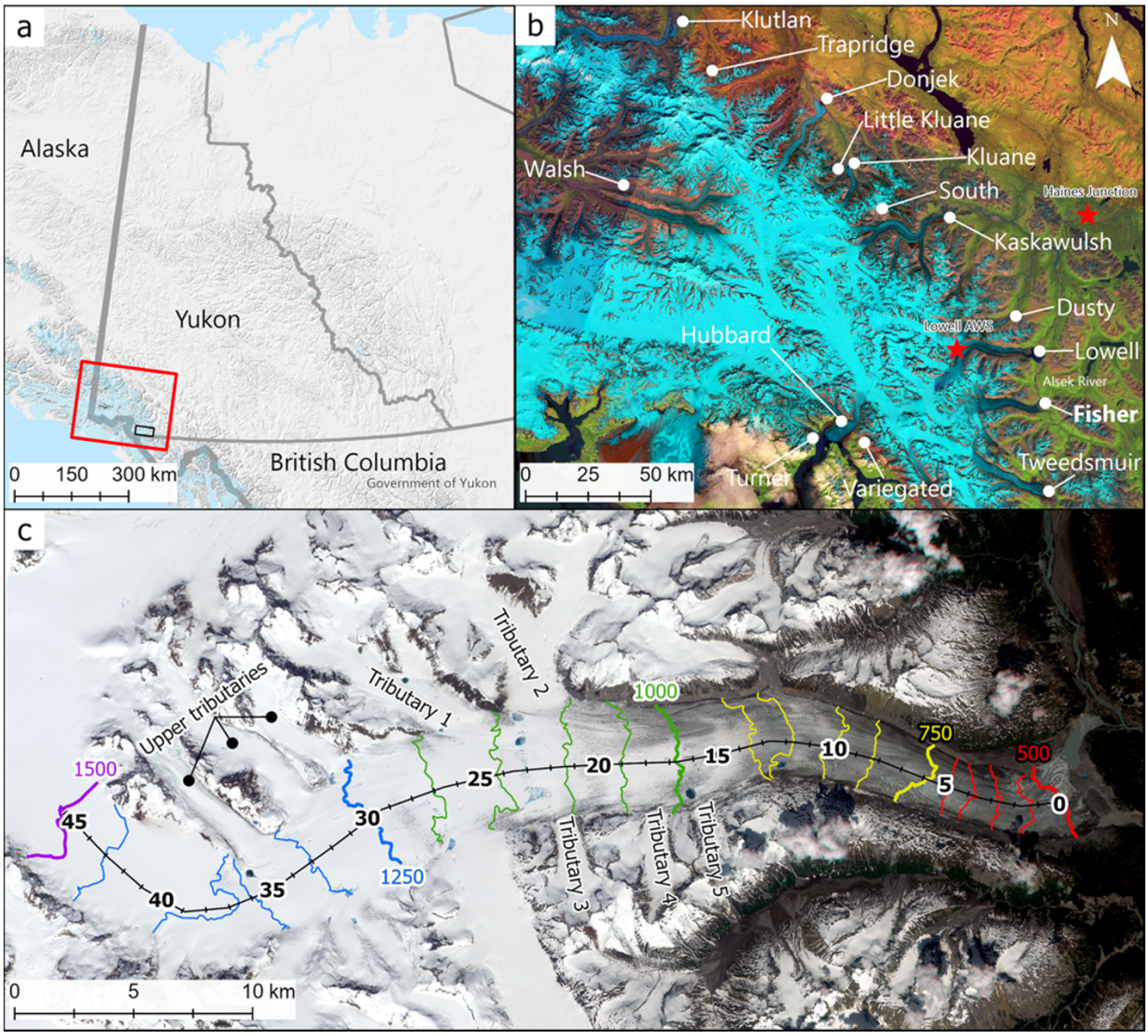

Figure 1. (a) Map of the Yukon outlining the areas covered by panels (b) (red) and (c) (black). Background: GeoYukon Map Services. (b) Location of Fisher Glacier (bold) and other glaciers referred to in the text. Red stars indicate the Haines Junction weather station and the Lowell Glacier automatic weather station (AWS). Background: Landsat image mosaic from August 2017 and July/August 2022. (c) Overview of Fisher Glacier, with black line marking centerline and km markers indicating distance from 2015 terminus. Colored contour lines show 50 m hypsometry bands on the main glacier trunk, with each color representing a 250 m elevation range. Base image: RapidEye-1, 22 June 2016.

The georeferencing error was calculated by measuring the offset between stable ground features located near the terminus on the air photos or declassified imagery and PlanetScope image from 4 July 2022. For the declassified imagery, this was 119.25 m for 1963 and 31.25 m for 1977, while for the RCAF air photos it was 32.67 m for 1948, 85.75 m for 1954, 60.25 m for 1972 and 20.14 m for 1976. In relation to image resolution, a conservative maximum uncertainty of ±2 pixels was used as an estimate for terminus delineation (Kochtitzky and others, 2019; Lauzon and others, 2023), assuming that errors resulting from manual terminus delineation are random. This corresponds to 120 m for Landsat 1–4, 60 m for Landsat 5, 30 m for Landsat 7, Landsat 8 and ASTER, 20 m or 40 m for SPOT 1–5 (depending on the image), 10 m for RapidEye 1–5, 6 m for PlanetScope, 15 m for the 1977 KH-9 image and ~280 m for the 1963 KH-5 image. For the historical air photos from 1948, 1954, 1972 and 1976, this equates to 2.94, 5.24, 6.12 and 7 m, respectively.

Uncertainties for the terminus advance and retreat calculated by the GTT toolbox were then calculated using the formula (after Hall and others, 2003):

$$\textit{Uncertainty} = \frac{\sqrt{(\textit{pixel length})^2 + (\textit{pixel width})^2} + \textit{georectification error}}{\textit{number of years}} \quad (1)$$

The pixel length and width in Equation (1) were calculated as the mean pixel size for both images involved in the calculation.

Changes in terminus area were calculated by creating polygons of the digitized termini, and time series of terminus area change were plotted to show the evolution through a full surge cycle.

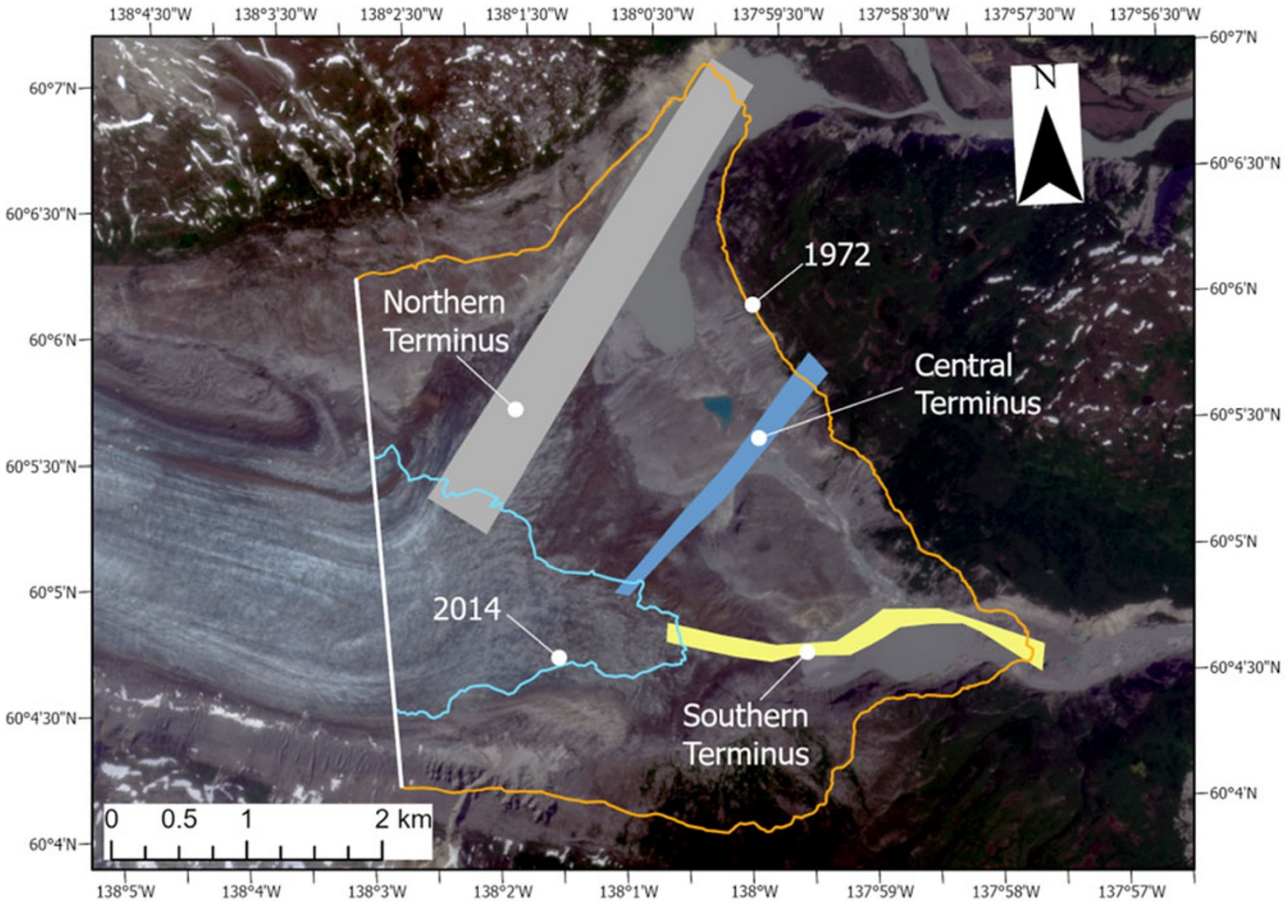

Figure 2. The three subsections on which the Glacier Termini Tracking toolbox was run (shaded areas), along with two examples of terminus polygons showing the maximum (1972) and minimum (2014) extents over the study period. The straight white line indicates the common line to which all terminus extents were clipped. Base image: PlanetScope, 4 July 2022.

Following methodology developed by Krumwiede and others (2014), uncertainties for area changes (A_{er}) were assumed to be ±1 pixel and calculated from the following equation:

$$A_{er} = (n \cdot m) \quad (2)$$

where n is the number of pixels that make up the perimeter of the terminus area (approximated by dividing the outline length by the image pixel size) and m is the spatial resolution of the sensor bands expressed as the area of a pixel (e.g. 900 m^2 for a 30 × 30 m pixel).

3.2. Surface velocities

Surface velocities of Fisher Glacier from 1985 to 2018 were primarily obtained from version 1 of the NASA Inter-mission Time Series of Land Ice Velocity and Elevation (ITS_LIVE) dataset (https://its-live.jpl.nasa.gov; Gardner and others, 2019). These are produced by the auto-RIFT feature tracking processing chain (Gardner and others, 2018), using optical imagery from Landsat 4, 5, 7 and 8. Files were downloaded and clipped to Fisher Glacier's outline, as defined by the Randolph Glacier Inventory version 6.0 (RGI Consortium, 2017).

Annual ITS_LIVE velocity mosaics at 240 m resolution were used for most periods, created from a weighted average of all available image-pairs that have a center date that falls within that calendar year (Gardner and others, 2018). Since the annual mosaics are composed of multiple scene pairs, they have lower uncertainties than the individual scene pairs but can miss details of velocity changes that occur over sub-annual periods. Therefore, velocity scene pairs at 240 m resolution (before 2013) and 120 m resolution (2013 and later) were used to derive short-term velocities for 2010 to 2016 during a period of rapidly changing speed. Filters for scene pair acquisition were set to a time separation of 14–120 days, with >30% coverage of the area of interest. The velocity pair results were then manually sorted and selected for best coverage both spatially and temporally, with a mean time separation of ~40 days for most image pairs. The uncertainty associated with the annual ITS_LIVE velocity mosaics is included with the downloaded product. For the individual scene pairs, the uncertainty was calculated as the average difference over bare ground.

Since optical image matching used in ITS_LIVE requires surfaces with distinctive features to track, it does not work well in the winter when the surface is typically snow-covered, sun angles are poor and daylight is limited. To derive winter velocities during the period of enhanced flow, we therefore used synthetic aperture radar (SAR)-based speckle tracking of RADARSAT-2 ultrafine data for 2014 to 2017, subsampled to 50 m resolution (Supplementary Table S2). SAR velocities derived from images collected in neighboring swaths within seven days of the original acquisition were combined to provide better spatial coverage across the glacier. In all cases, velocities for overlapping areas were nearly identical, so the mean velocity was used. In such cases, the dates referred to in the text are

the first date of the first velocity pair and the last date of the second velocity pair.

As it was not possible to derive glacier-wide velocity maps from the historical air photos for the pre-satellite era, point velocities were determined from manual tracking of the displacement of distinctive looped moraines and moulins or potholes between 1954 and 1976. The displacement of each feature was measured from the center of each moulin or pothole, and from the furthest point of successive loops for the looped moraines. In total, 10 moulins or potholes (near the glacier center) and four looped moraines (near the southern glacier margin) were identified and total displacement was measured for two periods: 1954–72 and 1972–76. Uncertainties associated with image resolution were calculated in the same way as for the terminus change described above (1.8 m for 1954–72 and 7.4 m for 1972–76). While this method provides a general idea of ice velocities during this time, the temporal resolution is poor and it is not possible to distinguish between quiescent and active phase velocities if both occurred during a single measurement period.

3.3. Interpretation of surface feature changes

During a surge, the surface of a glacier often changes significantly due to rapidly changing ice velocities and down-glacier transfer of mass. In this study, surface features on Fisher Glacier were identified visually in nadir satellite imagery and air photos (Supplementary Table S1), and traced out and tracked manually in ArcGIS Pro. A Gigapan (large panoramic) photo of the ablation zone was also taken from a bedrock knoll on the north side of the glacier (60°06′21.996″ N, 138°05′54.960″ W) on 11 August 2015, and repeated on 25 July 2021, which provided an oblique view of surface changes. Additionally, numerous oblique photos, taken with handheld cameras from a helicopter (2015, 2021) and Helio Courier aircraft (2021), offered views of the terminus and across the ablation area.

The timing of crevasse appearance, location, shape and extent on the glacier surface were used to provide insight into ice dynamic processes and a means to narrow down surge initiation and termination times and locations. The drainage of supraglacial lakes is also connected to crevasse formation and changes in basal water pressures (Murray and others, 2003), and was assessed visually to help reconstruct surge timing. As potholes are associated with the quiescent phase of the surge cycle (Meier and Post, 1969; Liestøl and others, 1980; Sturm, 1987), their evolution on the glacier surface was characterized using available imagery. This visual analysis is of particular importance in identifying older surges which occurred during times when glacier velocities and surface elevation changes were difficult, or impossible, to determine.

3.4. Surface elevation changes

3.4.1. Historical DEMs from air photos

The historical air photos from 1954, 1972 and 1976 (Supplementary Table S1) were used to create high-resolution orthoimages and DEMs of Fisher Glacier using Structure from Motion (SfM), following the methodology of Medrzycka and others (2023). Agisoft Metashape Professional was used to process the scanned images for SfM analysis after any poorly focused or overexposed scenes had been removed, which was common over snow-covered areas at higher elevations. Sixteen photos were used for the 1954 DEM, 17 photos for the 1972 DEM, and 16 photos for the 1976 DEM. The 1954 and 1976 DEMs cover the area up to ~27 km from the terminus, whereas the 1972 DEM covers the area up to ~35 km from the terminus. Masks were manually added to the photos in Metashape to remove any non-desired objects such as borders or marks on the scanned image caused by dust and dirt. The fiducial marks on the photos were defined, and each image was typically assigned a minimum of five GCPs on stable ground defined from cloud-free 3 m resolution PlanetScope images from 4 July and 12 August 2022. All GCPs (19 for 1954, and 31 for both 1972 and 1976) were placed on at least two images, with horizontal coordinates derived from the PlanetScope images, and elevations (in m a.s.l.) from the 2 m resolution ArcticDEM v3 mosaic (https://www.pgc.umn.edu/data/arcticdem/; Porter and others, 2018). Following the initial photo alignment, three dense point clouds (one per year) were created and manually filtered, to remove any remaining outlier points. The final point clouds were then used to create 3D models which were exported as DEMs, and orthophotos projected to WGS 1984 UTM Zone 7N.

3.4.2. Satellite-derived DEMs

Existing satellite-derived DEMs of Fisher Glacier were acquired from two ArcticDEM v3 strips at 2 m resolution, and the ASTER GDEM v3 (https://asterweb.jpl.nasa.gov/gdem.asp) at 30 m resolution. In addition, we created DEMs from 70 ASTER stereo satellite images covering Fisher Glacier and its surroundings. Images were selected with <80% cloud cover and daytime acquisition, downloaded in Level 1A format. These images were converted to DEMs using the MicMac ASTER MMASTER processing chain (Girod and others, 2017), which offers an accuracy better than ±10 m and minimizes the jitter-induced bias that affects ASTER imagery. The DEMs were manually inspected to remove those containing visible noise due to cloud cover or bad lighting, and the highest quality DEM from each year was selected. This process yielded a total of nine DEMs that were sufficiently noise-free, from 11 September 2003, 11 July 2004, 17 July 2006, 25 September 2014, 10 June and 14 July 2016, 4 July 2018, 16 July 2019 and 16 July 2020. The two 2016 DEMs each covered only about half of the glacier: one covering the top and the other the bottom. Since the acquisition dates of both DEMs were close, and elevation differences in overlapping areas were negligible, they were combined to provide a single DEM for 2016 with glacier-wide coverage.

3.4.3. DEM co-registration and trend analysis

Once the historical air photo and MMASTER DEMs had been created they were iteratively co-registered using a Python package (https://github.com/iamdonovan/dem-coregistration), based on the co-registration algorithm developed by Nuth and Kääb (2011). Prior to co-registration the DEMs were resampled to 30 m to be consistent with the ASTER GDEM v3. Some of the DEMs required additional filtering prior to co-registration to remove smaller patches of noise, which was accomplished by differencing them from the ASTER GDEM v3 and then filtering for values over a certain threshold. For the MMASTER DEMs, the threshold was set at 100–125 m (depending on the DEM). For the air photo DEMs, the threshold value was set at 200–250 m to account for greater errors in this data source and a longer time separation between the differenced DEMs.

Once co-registration was completed, trends in surface elevation change were computed using the make_stack.py script from the pygeotools Python package (https://pygeotools.readthedocs.io). The tool uses a 'stack' of rasters to create a raster showing the change in elevation standardized to values of m a^{-1}. It requires

at least three DEMs, which allows it to reduce uncertainties by calculating apparent change over stable ground and adjust the corresponding change over the glacier surface. Trends in surface elevation change were computed for three periods: 2003–14, 2016–20 and 2003–20, to enable quantification of elevation differences around a period of rapid glacier change in 2014–16. Since make_stack.py requires multiple DEMs from different years it was not used for the air photo DEMs, nor for the MMASTER DEMs covering the period of rapid glacier change from 2014 to 2016 since there were only two DEMs available (one for 2014 and another for 2016). In these two cases, the DEMs were differenced using the *Minus* tool from the *Spatial Analyst* toolbox in ArcGIS Pro, and the resulting DEMs of difference were filtered and standardized to annual values. Uncertainties were measured by calculating the mean value over stable ground (0.03 m a^{-1} for 1954–72, 0.32 m a^{-1} for 1972–76, 0.27 m a^{-1} for 2003–14, 5.58 m a^{-1} for 2014–16, 1.45 m a^{-1} from 2016–20 and 0.34 m a^{-1} from 2003–20).

4. Results

4.1. Terminus length and area changes from 1948 to 2022

Fisher Glacier's terminus retreated over most of the study period, punctuated by two short periods of rapid advance (Figs. 3 and 4). Historical air photos and declassified satellite imagery from 1948 to 1963 show that the terminus length and area of Fisher Glacier decreased steadily over this time (Figs. 3a and 4a), with a total reduction in area of 3.03 ± 1.85 km^2.

Between 1963 and 1972, the terminus area increased by 5.81 ± 1.89 km^2, reaching 15.86 ± 0.06 km^2 in 1972, the largest over the study period (Fig. 3). Over this period, the glacier also increased in length by an average total of 571 m, but this was highly spatially variable (Fig. 4b). The south terminus increased by >1900 m and the north terminus by >1400 m, but the central terminus only increased by <200 m. However, based on Fisher Glacier's recent behavior and the nearly 9 year gap in image availability, it is likely that the advance lasted for a shorter period, and that the advance amounts are minimums if the glacier started to retreat prior to 1972.

Over the following ~42 years, the terminus retreated at a fairly constant rate, until it reached its minimum extent on 31 July 2014 (Fig. 3a). Over this period, Fisher Glacier attained a terminus-wide average change of −2.05 km (Figs. 3b and 4c). As with the prior advance, this retreat was spatially variable, with the northern section retreating the most and central section retreating the least. The surrounding topography of each section is quite different, with the central being land-terminating and, at its maximum extent, the glacier terminus pushing up against an ~300 m high hill. In contrast, both the northern and southern sections are water-terminating, although the north terminates in deeper water in a permanent lake, whereas the south terminates in seemingly shallower water (Fig. 4d).

In summer 2014, Fisher Glacier's terminus began a new period of advance that would last for the next ~2 years (Figs. 3b and 4d). Between 31 July and 2 September 2014, the terminus experienced a rapid but small advance of an average of 18 ± 78 m, although some areas such as the north terminus were still retreating. This advance corresponded to a 0.13 ± 0.08 km^2 area increase. The rate of advance then slowed but remained above zero through the fall and winter of 2014–15. The first significant terminus advance occurred between 21 May and 23 June 2015, although it was mainly constrained to the northern section. After May 2015 the rate of change began climbing steadily through the summer and fall of 2015, reaching a peak in winter 2015–16. The fall and winter of 2015–16 is when the terminus experienced its greatest change, advancing by an average of 526 ± 20 m between 4 October 2015 and 10 May 2016, with the greatest advance in the northern section (1236 ± 20 m). The rate of advance remained high throughout early summer 2016, until sometime between 18 July and 21 August 2016 when it rapidly dropped and the terminus became stagnant, or showed very slight retreat, until 6 August 2017.

The period of rapid change lasted for a total of ~2.1 years (31 July 2014 to 21 August 2016), during which the terminus increased in area by a total of 5.41 ± 0.23 km^2. By 2017, terminus area changes returned to being negative, with this trend being maintained to the end of the study period in summer 2022 (Figs. 3a and 4e).

4.2. Velocity changes from 1954 to 2022

Manual tracking of surface features from historical air photos from 1954, 1972 and 1976 provide point surface velocities in the mid-region (ablation area) of the glacier, ~10–20 km from the terminus (note that all calculated distances are measured from the 2015 terminus, as shown in Fig. 1c). Potholes and moulins located along the glacier centerline progressed down-glacier by an average of 233 ± 1.8 m a^{-1} from 1954 to 1972. Their displacement then decreased to an average of 22 ± 7.4 m a^{-1} from 1972 to 1976. Due to the lack of detail concerning how velocities varied during 1954 to 1972, it is likely that short-term velocities were much higher during at least one part of this period if a surge occurred.

NASA ITS_LIVE average annual velocity mosaics show that surface velocities gradually increased along the centerline, though remained generally low (ranging from <50 to 90 ± 14 m a^{-1}), from 1985 to 2010 (Fig. 5). Over this time, the mean annual centerline velocity increased by a few meters per year (Fig. 5b). Figure 5a illustrates the gradual up- and down-glacier spread during this multidecadal slow velocity increase. Between 2011 and 2012, average velocities started increasing more rapidly (Fig. 5b), with the speedup in 2011 occurring in the central ~20 km of the glacier (Fig. 6). This region of high velocity expanded to encompass a larger part of the glacier over the next couple of years, with the speedup increasing substantially in 2014 and 2015 as Fisher Glacier began a period of rapid acceleration.

The annual centerline velocities increased yearly since 1985, starting at the 25 km mark and slowly spreading up- and down-glacier (Fig. 7a). The increase is very gradual at first, with higher speeds starting around 2008, when they surpassed 100 ± 60 m a^{-1} in the region from 22 to 29 km from the terminus. In Fig. 7a, the following years' peak velocities (i.e. 2009) can be seen slowly increasing, both up- and down-glacier from where they first started. In 2012, they passed the 150 ± 102 m a^{-1} mark, in 2013 they climbed above 200 ± 52 m a^{-1}, and by 2015 they reached >600 m a^{-1}.

The short-term velocity data obtained from ITS_LIVE and SAR sources show further detail concerning the evolution of velocities throughout the period of rapid surface movement that lasted from 2013/14 to 2016. After velocities started to accelerate in 2014, they rapidly increased throughout spring 2015 (February to April), and by late summer and fall 2015 the entire length of the glacier was flowing at an average of ~1000 m a^{-1}. The winter and spring of 2016 are when the greatest velocities occurred: between 7 February and 9 March 2016, the rapid velocities finally reached the terminus,

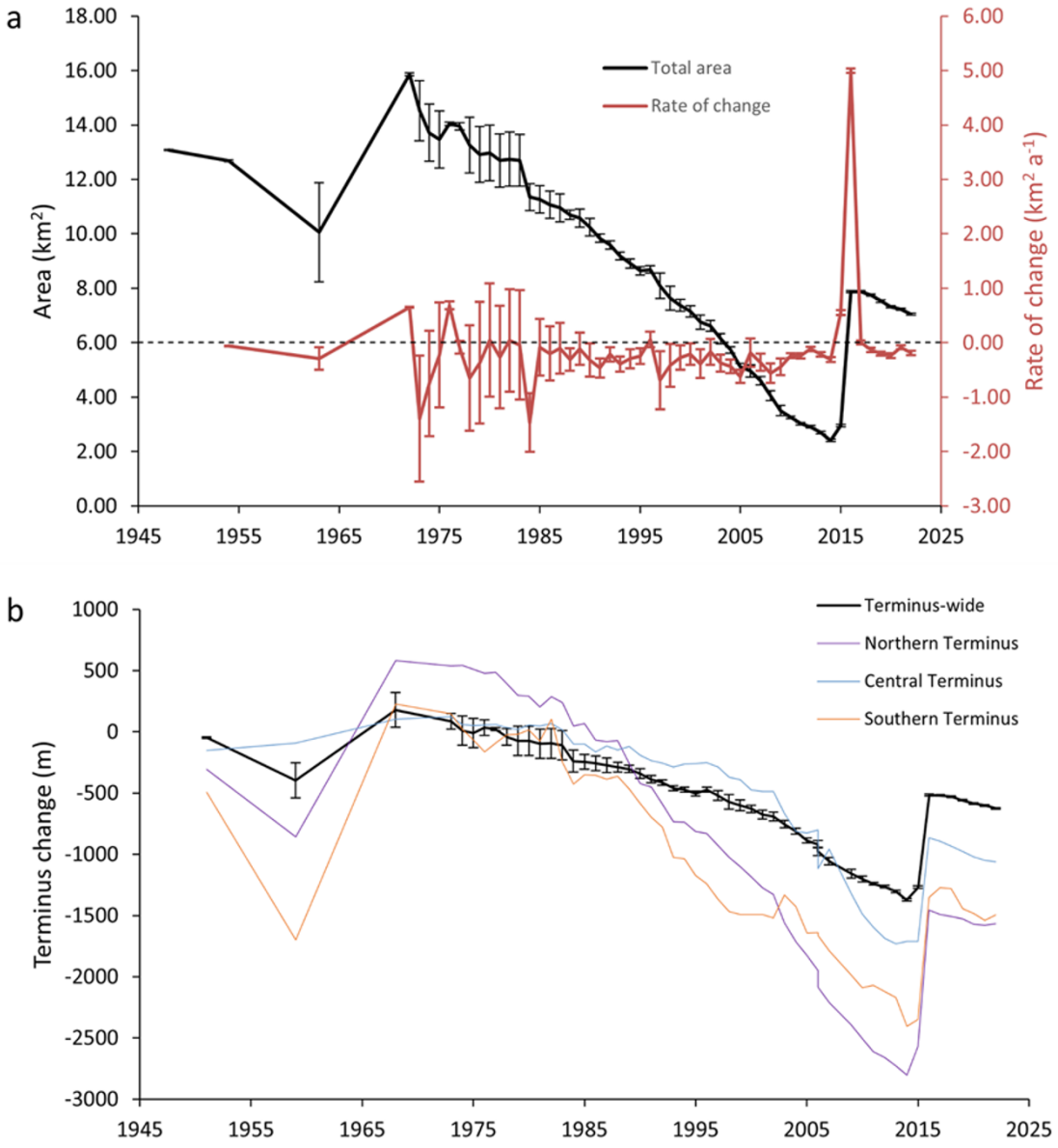

Figure 3. Time series of (a) total terminus area (black line) and annual rate of change (red line) for Fisher Glacier from 1948 to 2022; (b) change in terminus length in relation to its 1948 extent; error bars are only included on the terminus-wide line because they are the same for all lines.

which had previously remained below 100 m a^{-1}. At this time, the terminus attained a mean velocity of ~700 m a^{-1} and increased to a mean of >1100 m a^{-1} from March 2 to 26, 2016. February 2016 also marked the time where the upper glacier reached its observed peak speeds, with enhanced velocities reaching >41 km up-glacier from the terminus, affecting approximately 91% of Fisher Glacier's length (Figs. 6 and 7a). Velocities remained high throughout the early summer of 2016 with a peak of 2157 m a^{-1} recorded between 13 May and 6 June 2016, around 12 km from the terminus.

At the end of June 2016, flow speeds in the mid-glacier (12–21 km) dropped by ~1000 m a^{-1} in the span of a month (from a mean of 1758 m a^{-1} in early June to 735 m a^{-1} in July). Between July and September 2016, the velocities dropped again, this time to a mean of 162 m a^{-1} in the mid-glacier. By January/February 2017 the mean ice velocity was only 34 m a^{-1}, and this remained similar through 2018. ITS_LIVE point data from 2017 to 2022 shows that Fisher Glacier undergoes regular midsummer speedups (Fig. 7b), but these are short-lived and the mean velocity during the rest of the year remains low (<50 m a^{-1} from 2017 to 2022).

4.3. Surface feature changes

4.3.1. Surface feature changes between 1948 and 2010

In the 1948 and 1954 historical air photos the glacier surface appears smooth, and in 1954 potholing is present from ~15 km from the terminus to at least 30 km up-glacier, beyond which no imagery is available (Fig. 8a). By 1972, nearly all the potholes had disappeared due to extensive new crevassing that covers the glacier, with only a few of the largest still visible (Fig. 8b). In the lower ~7 km of the glacier, crevasses were widespread across the entire ice surface at this time, whereas above this some areas were less crevassed, although not completely unaffected. Additionally, the ice margins across the lower glacier, which were in a state of down-wasting in 1954, are bulging out in 1972 (Fig. 8b). Furthermore,

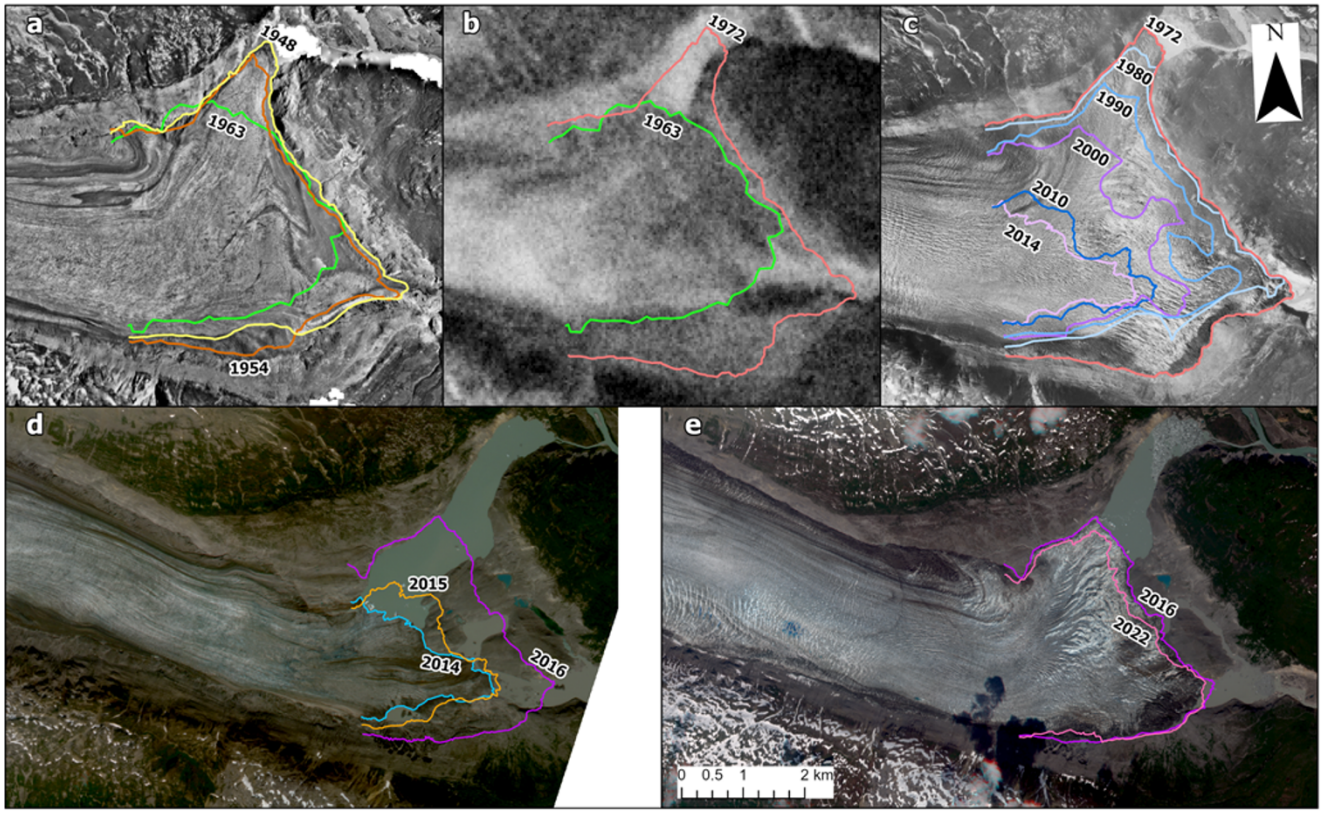

Figure 4. Terminus extents during Fisher Glacier's periods of advance (b, d) and retreat (a, c, e) between 1948 and 2022: (a) Retreat from 1948 to 1963. Base image: 12-06-1948 air photo. (b) Advance from 1963 to 1972. Base image: KH-5 image from 29-08-1963. (c) Retreat from 1972 to 2014, with decadal terminus outlines showing retreat patterns. Base image: Air photo from 08-08-1972 at the glacier's maximum documented extent. (d) Advance from 2014 to 2016. Base image: RapidEye-3 image of Fisher Glacier's minimum extent on 31-07-2014. (e) Retreat from 2016 to 2022. Base image: RapidEye-1 image from 22 June 2016. All images are presented at the same scale.

the texture of the snow up to 33 km from the terminus, and on the upper tributaries, suggests the presence of snow-covered crevasses in the upper glacier in 1972.

Images from 1976 and 1977 show that the glacier surface had smoothed out, although remnants of large crevasses from 1972 were still present along the glacier margins and at the terminus (Fig. 8c). It did not take long for the potholes to reappear, because in 1977 >100 small potholes were already present, although they were smaller and less extensive than in 1954. As of 1984, potholes now extended far above the snowline to 37 km from the terminus, and they remained extensive in the mid-1990s (Fig. 8d), but had reduced by the early 2000s.

4.3.2. Surface feature changes between 2010 and 2021

The period ~2014 to 2016 was marked by a series of rapid and pronounced surface feature changes. The potholes and associated surface ponds, still numerous in 2010, almost entirely disappeared or drained between 2011 and 2014. At the end of July 2014 (i.e. date of minimum terminus extent), a RapidEye-3 image shows that the glacier surface was still smooth throughout its entire length (see part of the glacier surface in Fig. 4d). Extensive crevassing began spreading across the lower glacier during winter 2014–15, or in spring 2015, as crevasses opened from the terminus up to ~15 km up-glacier. At this point, the crevasses were mostly located along the glacier margins. Field observations confirm the extensive crevassing in the lower ablation area and terminus (Fig. 9), with the glacier's surface very broken up and characterized by undulating hills on a surface that is typically smooth and flat when not surging (Figs. 9c and d). Large seracs were also observed both at the terminus (Fig. 9a) and up-glacier in the lower ablation area (Fig. 9f). The terminus was heavily fractured and terminated in the northern proglacial lake with a defined ice cliff as a calving front (Fig. 9a). By the end of summer 2015, the large crevasses at the terminus and along the margins in the ablation zone were generally about 20–30 m wide. The smaller crevasses, which at this point were generally found toward the center of the trunk, measured a maximum of about 8–12 m in width.

Crevasse formation was amplified across most of the glacier between summer 2015 and summer 2016. RapidEye-1 imagery from 22 June 2016 shows very large crevasses and serac formation at the terminus, with crevasses generally measuring 20–40 m at their widest point, although some reached widths of >60 m (Fig. 4e). The crevasses up-glacier from the terminus had now spread across the entire glacier width in most areas and extended up to 37 km up-glacier from the terminus, similar to 1972. This included intense crevassing on the tributaries high in the accumulation zone. By 2021, the ice was much smoother, and only crevasse remnants can be distinguished on the surface (Figs. 9b and d). In 2021, potholes reappeared (Fig. 9g), covering an extensive region where potholes used to be located prior to 2011 (Fig. 8f).

4.4. Surface elevation changes from 1954 to 2022

Elevation changes derived through DEM differencing of historical images show that from 1954 to 1972 the area of Fisher Glacier below 1050 m a.s.l. experienced thickening at an average rate

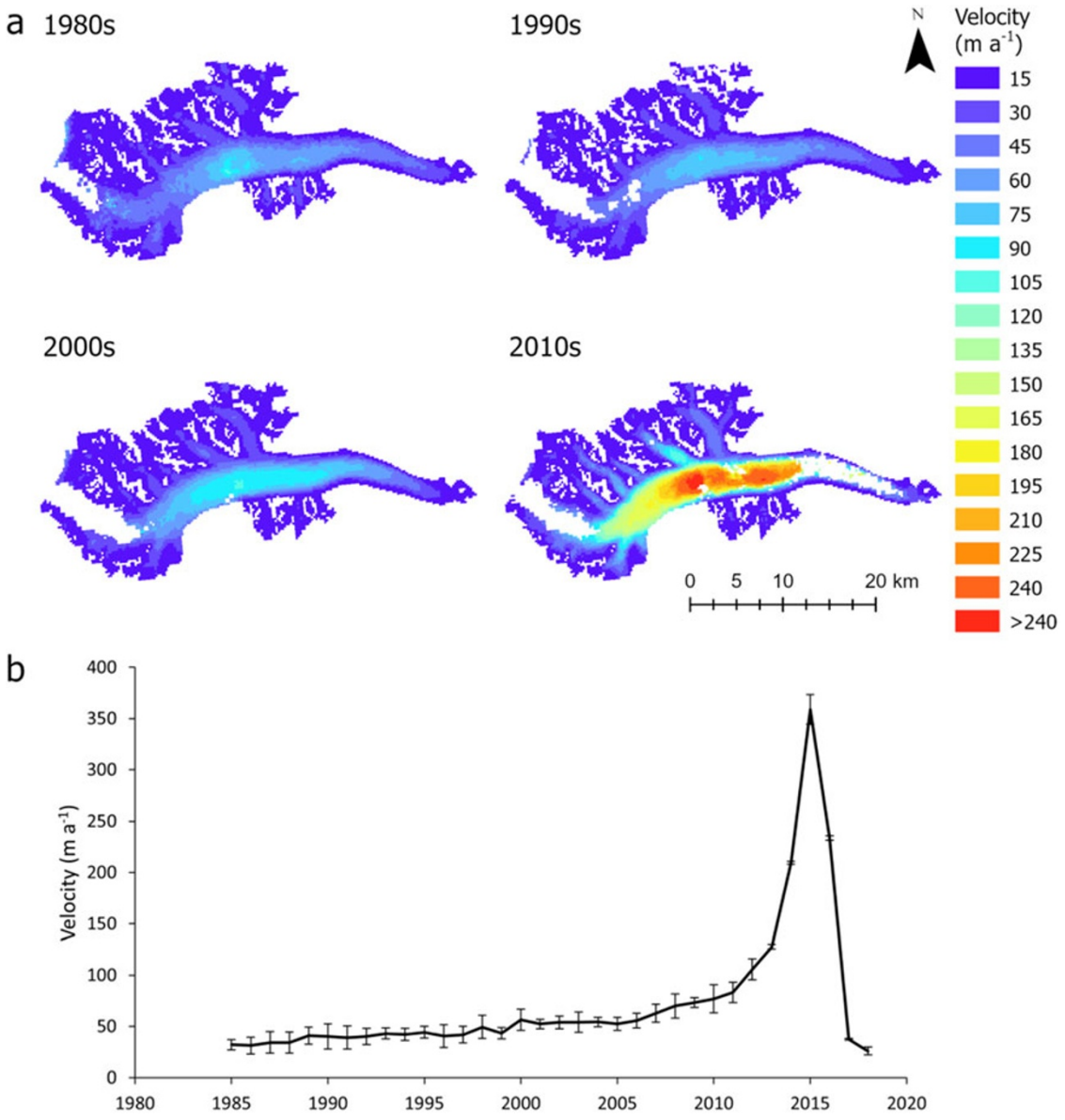

Figure 5. (a) Decadal surface velocity mosaics (m a^{-1}) of Fisher Glacier covering the period 1985–2018 (1980s = 1985–89; 1990s = 1990–99; 2000s = 2000–09; 2010s = 2010–18). These mosaics display the mean velocity derived from all ITS_LIVE annual mosaics available for each decade. (b) Average annual centerline velocity (1985–2018) of Fisher Glacier, calculated from the mean of all cells within 500 m on either side of the centerline over a distance of 0–45 km up-glacier from the 2015 terminus. Figure 1c shows the centerline.

of + 1.70 ± 0.03 m a^{-1}, while the surface area above 1050 m a.s.l. lowered at an average of −1.45 ± 0.03 m a^{-1} (Fig. 10a). The dynamic balance line (DBL), defined as the location where surface elevation change switches from positive to negative (Dolgoushin and Osipova, 1975), was located at 19.9 km from the terminus for 1954 to 1972. The trends in ice volume change follow a similar pattern to the elevation change trends (Fig. 10b), with the area above 1050 m a.s.l. undergoing a mean volume loss of −0.02 km^3 a^{-1} from 1954 to 1972.

From 1972 to 1976, the historical DEM of difference shows that nearly all 50 m hypsometry bands had a negative surface elevation change (Fig. 10a). With that said, the elevation bands at higher elevations were subjected to the greatest thinning rates: The elevation bins from 450-950 m a.s.l. lowered by an average of −3.10 ± 0.32 m a^{-1}, whereas the elevation bins above 950 m a.s.l. lowered by an average of −5.79 ± 0.32 m a^{-1}. This resulted in the greatest volume loss occurring in the upper parts of the glacier (an average of −0.072 km^3 a^{-1} above 950 m a.s.l. compared to −0.018 km^3 a^{-1} below 950 m a.s.l.; Fig. 10b).

The next available DEMs are the MMASTER DEMs covering 2003 to 2020. From 2003 to 2014, the DBL was located at 31.5 km up-glacier from the terminus, with the area above this (at >1250 m a.s.l.) increasing in surface elevation at an average rate of + 2.37 ± 0.27 m a^{-1} (Figs. 10c and 11a). This translated to an average annual volume gain of 0.058 km^3 a^{-1} above the DBL (Fig. 10d). The area below the DBL lowered at an average rate of −1.88 ± 0.27 m a^{-1}, although the volume loss from 450–1000 m a.s.l. was only slightly negative.

Following this, the elevation change map from 2014 to 2016 shows a down-glacier transfer of mass from above the DBL (1300 m

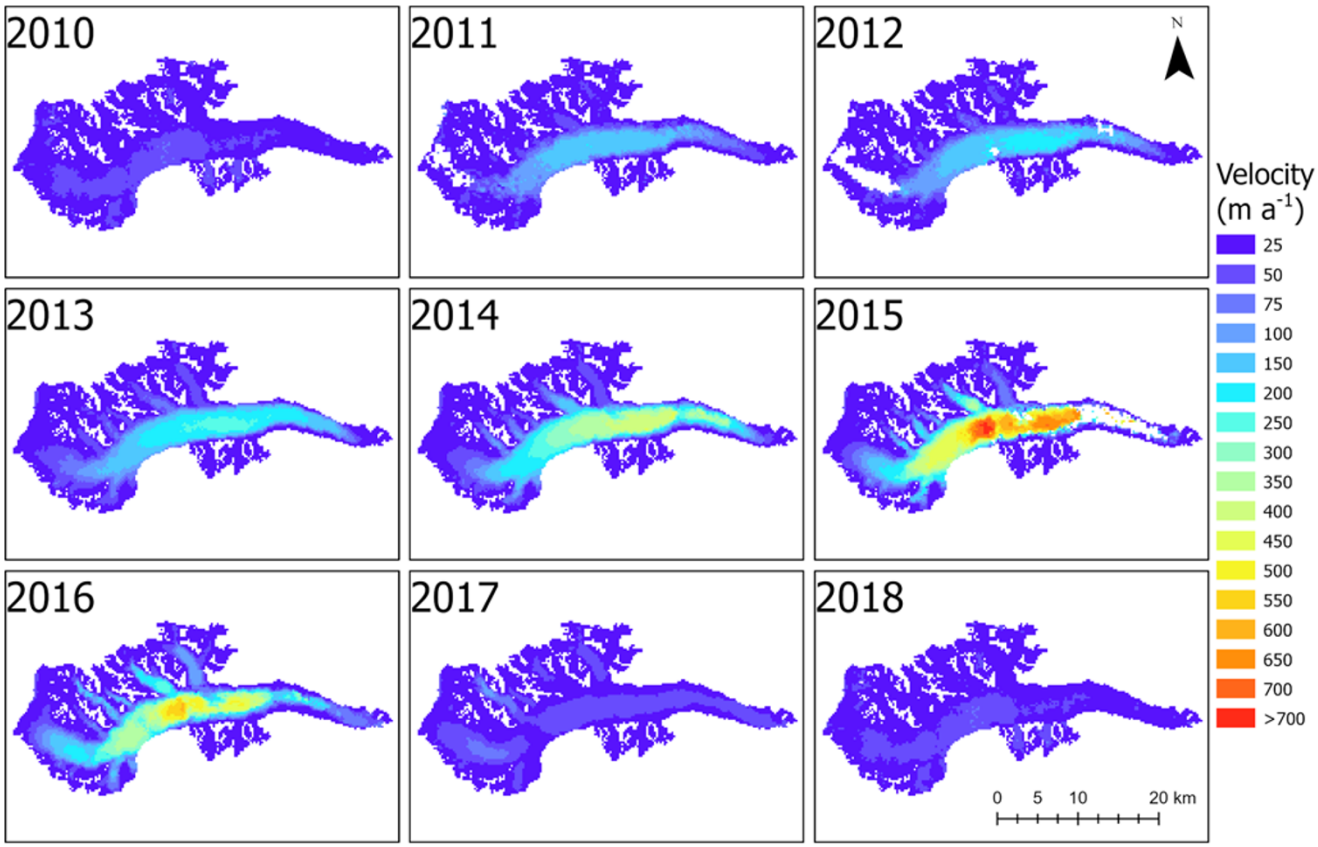

Figure 6. Annual surface velocity mosaics (m a^{-1}) of Fisher Glacier covering the period 2010–18, derived from ITS_LIVE data (Gardner and others, 2019).

a.s.l.; 31.5 km) to the area below it (compare Fig. 11a and b). The area below 1300 m a.s.l. experienced an average surface elevation increase of 18 ± 5.58 m a^{-1}, although this varied spatially. The terminus and lower receiving zone (<700 m a.s.l.; 0–4.8 km from the terminus) raised by + 39.77 ± 5.58 m a^{-1}, while the lower- to mid-section of the glacier (i.e. area between 700 and 1270 m a.s.l., or 4.8–23.7 km from the terminus) only raised by + 9.41 ± 5.58 m a^{-1} (Fig. 11c). The surface elevation changes from the MMASTER difference DEMs suggest that the DBL moved up-glacier by ~11.5 km, rising by ~250 m in elevation, between the historical (1954 to 1972) and recent (2003 to 2016) periods.

From 2016 to 2020, Fisher Glacier started another period of widespread surface thinning, similar to what was observed after 1972. The glacier surface now displayed a negative rate of change over its entire length, with no evidence for mass gain in the reservoir zone. The thinning rates were more pronounced in the receiving area (Fig. 11c), and the greatest volume loss occurred at 1000 m a.s.l. (−0.119 km^3 a^{-1}; Fig. 10d). The lower half of the glacier (up to 22.7 km from terminus; <1100 m a.s.l.) thinned at an average rate of −6.94 ± 1.45 m a^{-1}, while the upper half displayed an average rate of −2.33 ± 1.45 m a^{-1}.

The overall surface elevation trend on the main trunk from 2003 to 2020 shows that the DBL was located at an average altitude of 990 m a.s.l., which corresponds to a distance of ~16 km from the 2015 terminus (Fig. 11d) and is very similar to the DBL for 1954 to 1972. This means that about 70% of Fisher Glacier's area is located above the DBL. End of summer snowlines from 2010 to 2022 suggest that the equilibrium line altitude (ELA) is located at a mean elevation of 1409 m a.s.l., ~38 km up-glacier from the terminus and nearly at the head of the glacier. The reservoir zone is thus located primarily in the ablation area. Over the entire 2003 to 2020 period, Fisher Glacier displays a glacier-wide net volume change of −5.14 ± 1.26 km^3. Figure 11d also shows that, while most of the mass comes from the upper reservoir zone and accumulation area of the main trunk, a few tributaries also contribute: in particular, Tributary 1 and the upper tributary both display elevated surface lowering rates compared to the other tributaries, and these were the same two that displayed the highest velocities from 2013 to 2016 (Figs. 6 and 11d).

5. Discussion

The results strongly suggest that Fisher Glacier underwent two surges between 1948 and 2022 that were separated by a ~40 year quiescent phase. In the following section, the most recent surge is discussed first as it is better constrained than the older one and can therefore provide insight into the changes that likely occurred in the older surge when less imagery and data are available.

5.1. Evidence for a recent surge from 2013 to 2016

Fisher Glacier experienced significant change over the period 2013–16, during which its velocities dramatically increased, mass was redistributed down-glacier, the terminus advanced significantly and the ice surface displayed a number of changes including crevassing, serac development and formation of new looped moraines.

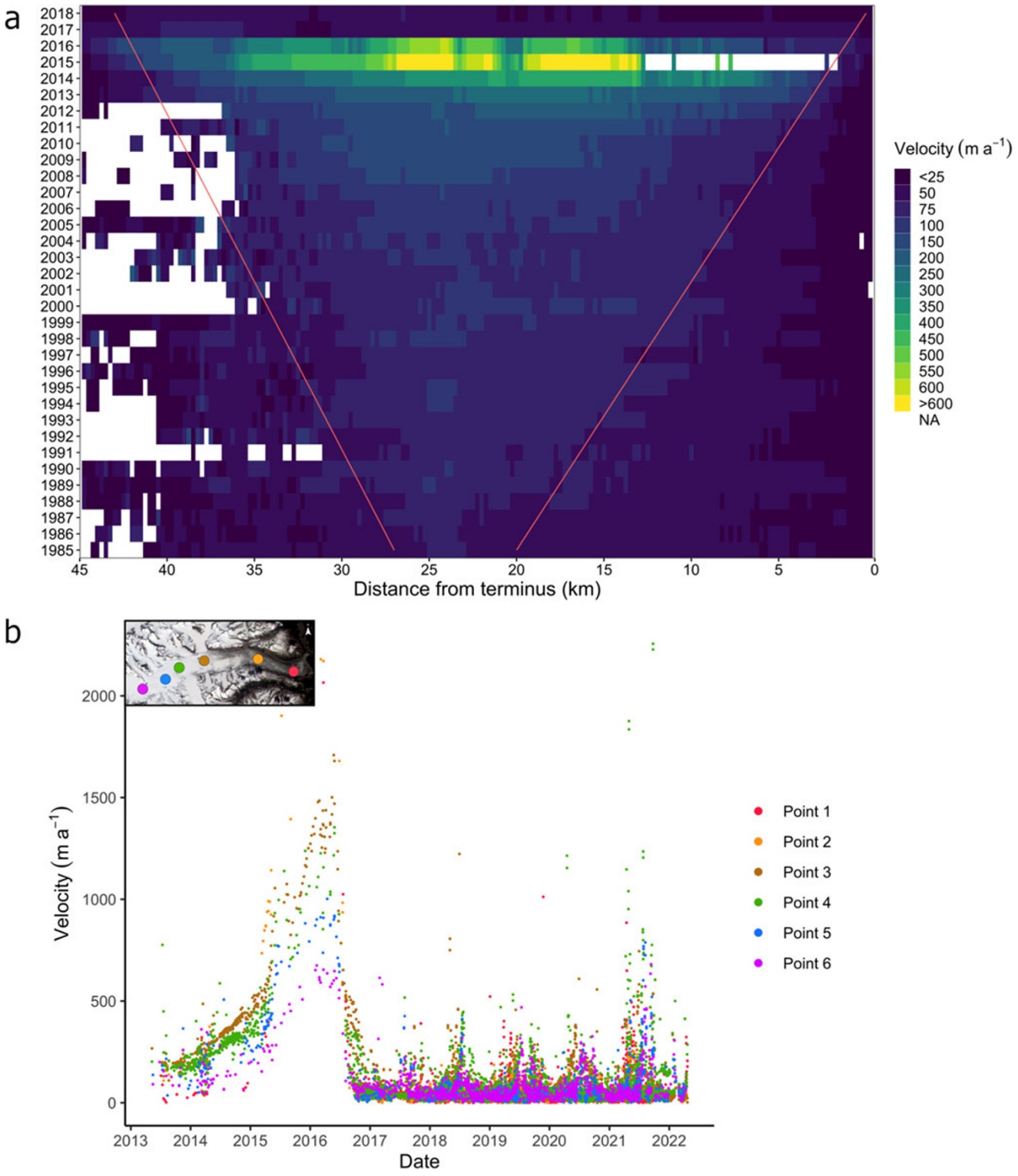

Figure 7. (a) Annual ice velocities from 1985 to 2018 in 250 m distance bins along the centerline of Fisher Glacier, extracted from ITS_LIVE annual mosaics (Gardner and others, 2019). Red lines are the approximate boundary between $<$50 and $>$50 m a^{-1}, showing the long-term patterns of the speedup starting from the middle part of the glacier. (b) Point velocities from 6 locations along the centerline of Fisher Glacier, derived from ITS_LIVE data (Gardner and others, 2019). Inset map shows the point locations with corresponding colors. Point locations 1–6 are located at 2, 10, 22, 27.5, 31.5 and 37 km from the 2015 terminus, respectively.

Velocity changes were the first sign of change on Fisher Glacier, appearing much earlier than the other tracked changes. The ice velocity displayed a very long and gradual increase through the 1980s to 2000s (at a rate of ~2 m a^{-1}), during which it increased both up- and down-glacier from the central part of the trunk, originating at a location around 24 km from the terminus. However,

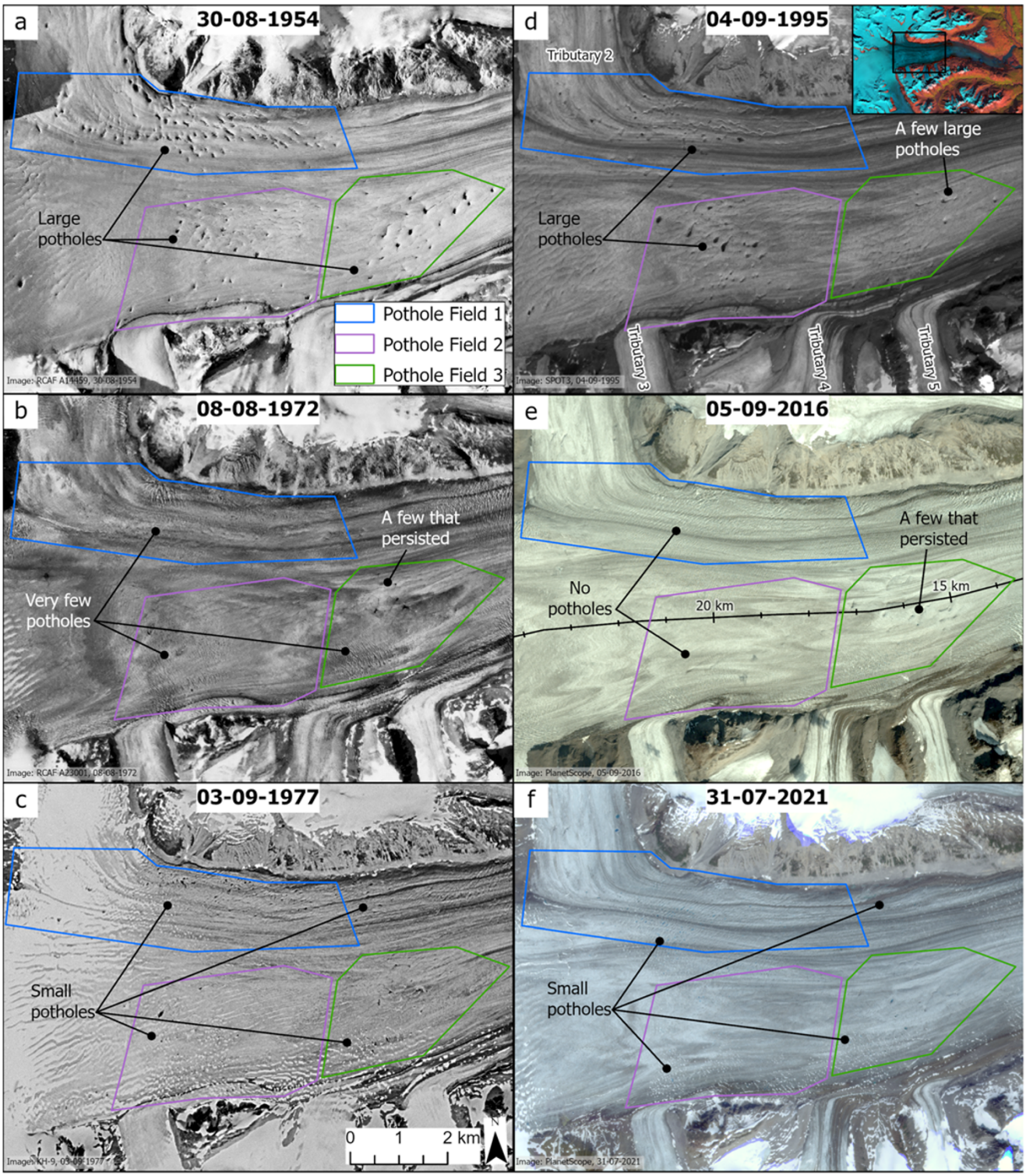

Figure 8. Evolution of potholes and crevasses on Fisher Glacier through two full appearance/disappearance cycles in three main pothole fields in (a) 1954, large potholes present; (b) 1972, almost no potholes; (c) 1977, small potholes reappearing; (d) 1995, large potholes; (e) 2016, almost no potholes (centerline distance markers shown on black line); and (f) 2021, small potholes reappearing. Inset map shows the location of the pothole fields near the mid-point of the glacier.

we still consider the glacier to be in its quiescent phase during this time as the flow was slow overall (ranging from <50 to 90 ± 14 m a^{-1}) and the terminus retreated on average by >2 km during this period.

It was only from about 2008 onward that the annual velocity began increasing at an enhanced rate (i.e. an annual rise of >2 m a^{-1}). 2007–08 marked the start of the pre-surge buildup when a localized region at the center of the glacier first began flowing

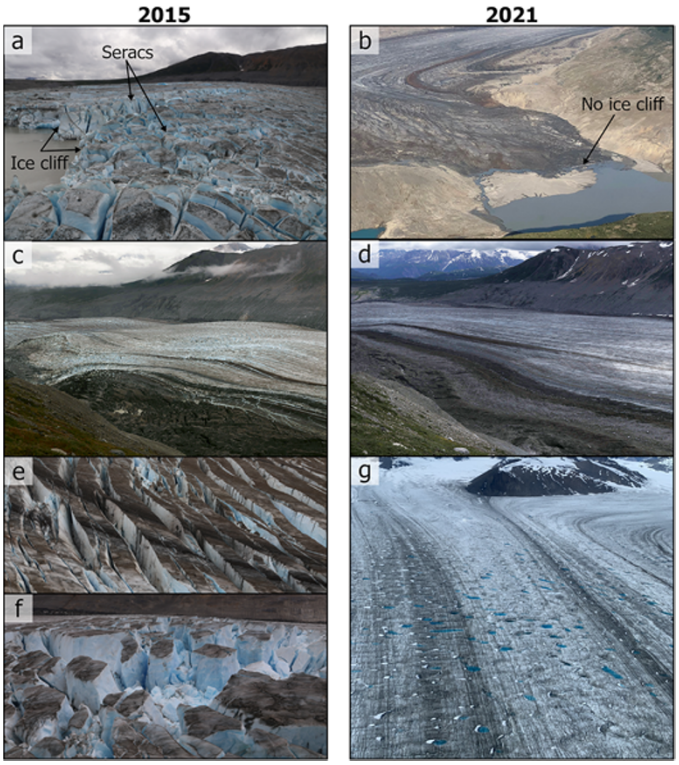

Figure 9. Surface feature changes of Fisher Glacier between 11-08-2015 (left column) and 25-07-2021 (right column): (a, b) Contrast between seracs and ice cliff where the terminus meets the proglacial lake along the northern section of the terminus (left), compared to a smooth surface in 2021 (right). (c, d) View across the lower ablation area, showing the contrast between a broken up, extensively crevassed and undulating surface in 2015 (left), compared to a smooth, flat and generally higher surface in 2021 (right). (e) Close-up of crevasses in the ablation area in 2015. (f) Close-up of seracs in the ablation area in 2015. Blue ice is indicative of recently exposed areas, suggesting an actively changing landscape. (g) Ponds formed in potholes on an otherwise featureless/flat surface, with Tributary 2 on the right.

>70 m a^{-1}. In 2010, the moderate flow speeds of the pre-surge buildup phase spread to a greater portion of the glacier, increasing up- and down-glacier from where they began in the central region. From 2008 to 2013 or so, most potholes, ponds and moulins that remained on the glacier surface drained or closed due to changes in the glacier morphology. The terminus, however, still showed consistent retreat with no sign of slowing. Additionally, the reservoir zone was still gaining elevation (mean 33 ± 4 m from 2003 to 2014), while the receiving zone was losing elevation (mean −26 ± 4 m from 2003 to 2014).

We consider the active phase of the surge to have begun in 2013 as the mean centerline velocities were >100 m a^{-1} with local flow speeds in excess of 200 m a^{-1} in the central region. However, the glacier surface remained visibly unchanged through 2013 and early 2014. The first visible signs of surging only became noticeable in late 2014, when the terminus began advancing very slowly as the surge front finally reached it. The first significant changes in terminus length and area came in early summer 2015, approximately coinciding with the time when the rapid velocities reached the terminus area. Spring/early summer 2015 is also when the glacier surface became heavily crevassed. Longitudinal crevasses were observed from ∼4 km down to the terminus where they splay outward, suggesting that the ice is being thrust upward there (Colgan and others, 2016). Seracs were also observed along the glacier margins and across the lower ablation area in regions where the ice became convex, which is a clear sign of active surging (Meier and Post, 1969; Hambrey and Alean, 2004). The advancing ice and down-glacier transfer of mass also created a new ice cliff at the advancing front. Additionally, the spring of 2015 saw the appearance of a number of supraglacial and ice-marginal lakes which subsequently drained through the summer during the same period that velocities increased in the lower glacier.

The velocities and terminus advance both peaked during winter or early spring of 2016, ∼2 years after the active phase initiated. Velocities reached a peak of >5.5 m d^{-1} (2100 m a^{-1}) from early February to early June 2016, at a distance of 8–12 km from the terminus. Correspondingly, the terminus was subjected to its greatest area change during this period, and crevasses kept growing and spreading across the glacier's surface. Our results are consistent with those of Altena and others (2019), who describe an increase in speed on Fisher Glacier from 2013 to 2018, and a down- and up-glacier propagation from the same surge initiation point that we identified at ∼22 km. However, their peak reported velocities of ∼4 m d^{-1} were lower than ours, likely because their results were more generalized at the glacier-wide scale. Guillet and others (2025, their figure 9, panel 4) show that the first clear increase in surface velocity of Fisher Glacier began approximately 1000 days (2.7 years) before the surge peak, aligning with our findings of the active phase beginning in late 2013 and peaking in mid-2016.

Velocities dropped rapidly at the end of summer 2016 within the space of only 1–2 months. The slowdown began at the same location where the surge had initiated (∼20–25 km from the terminus), and, as with the initiation, it also spread up- and down-glacier. The abrupt timing of the surge termination is also visible in Guillet and others' (2025) results. The following years were characterized by slow velocities (<50 m a^{-1}), surface lowering, and terminus retreat. The crevasses took a few years to close completely, but had mostly disappeared by 2021, and potholes had reappeared at the same location as before, which Sturm (1987) argues is a sign of quiescence.

5.2. Evidence for a historic surge ∼1970

The historic air photos and satellite imagery provide evidence for a surge that occurred shortly before 1972, supported by the observation of Clarke and Holdsworth (2002) that it had surged around 1970. The RCAF images from 1947, 1948 and 1954 all show a smooth surface that is devoid of crevasses, and an ice margin that

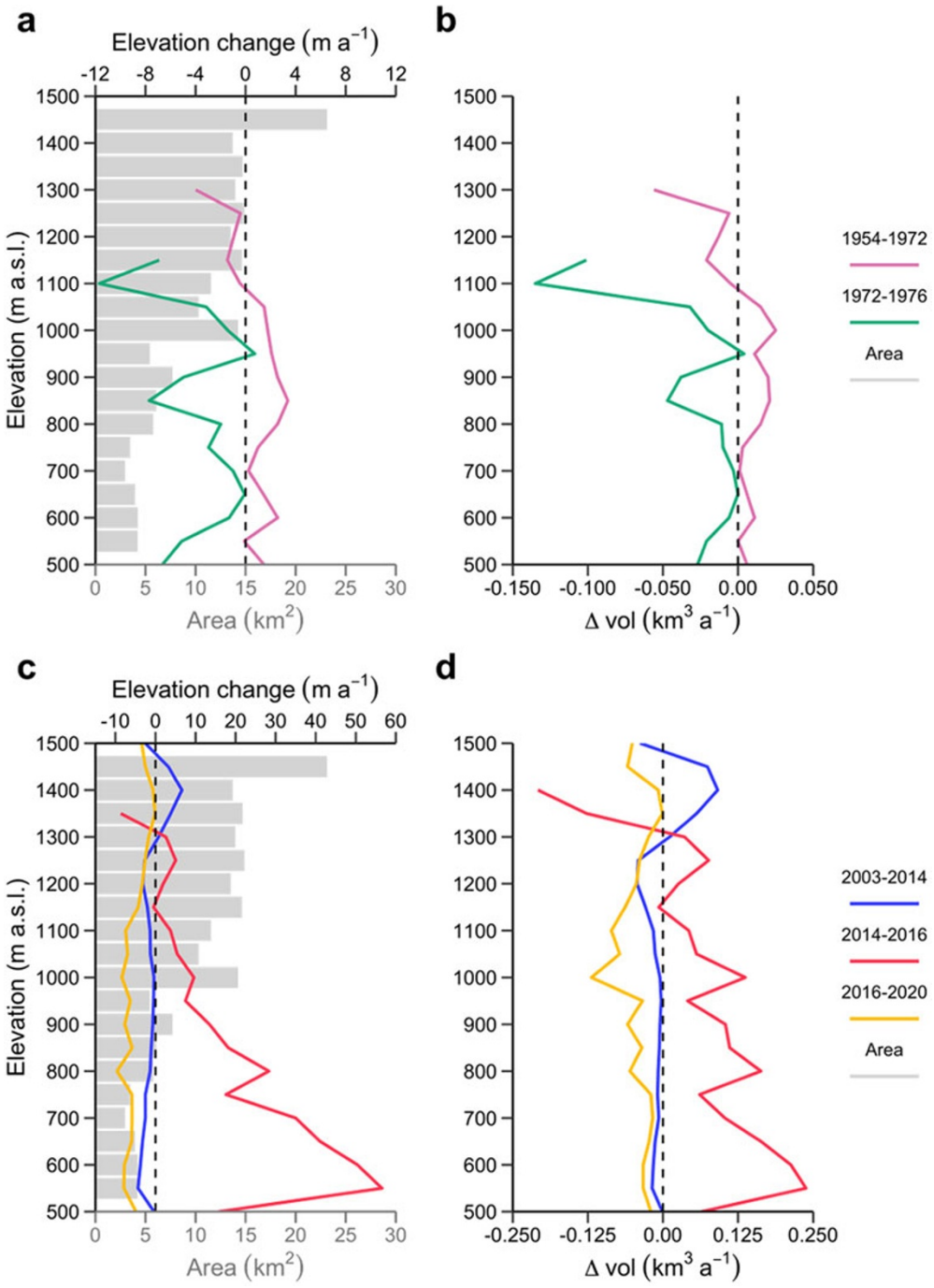

Figure 10. (a) Fisher Glacier hypsometry (grey bars) and average annual surface elevation change per 50 m elevation band for 1954–72 (pink) and 1972–76 (green). (b) Mean annual ice volume change per 50 m elevation band for the same periods as in (a). (c) Fisher Glacier hypsometry (grey bars) and average annual surface elevation change per 50 m elevation band for 2003–14 (blue), 2014–16 (red) and 2016–20 (orange). (d) Mean annual ice volume change per 50 m elevation band for the same periods as in (c). Note the difference in scales between (b, d).

is in a state of downwasting. The 1954 orthophoto, whose coverage extends further up-glacier than the 1947 and 1948 photos, also shows many large potholes covering the glacier surface above the 18–22 km mark. Additionally, the terminus length and area data show that the terminus had retreated and covered a smaller area between 1948, 1954 and 1963.

In 1972, the air photo shows a surface that is crevassed from the terminus all the way up to >30 km up-glacier, and a terminus more advanced than in 1963. A ~170 m high nunatak that was visible at the terminus in the previous images has been completely covered by ice, indicating a significant increase in ice volume there. The glacier surface in 1972 greatly resembles that of 2016 in terms of crevasse distribution and extent, and much like 2016, the crevasses at the terminus were chaotic, being oriented both in transverse and longitudinal directions, and forming serac fields. The appearance of a new looped moraine ~22 km up-glacier from the terminus further supports the occurrence of a surge during this time.

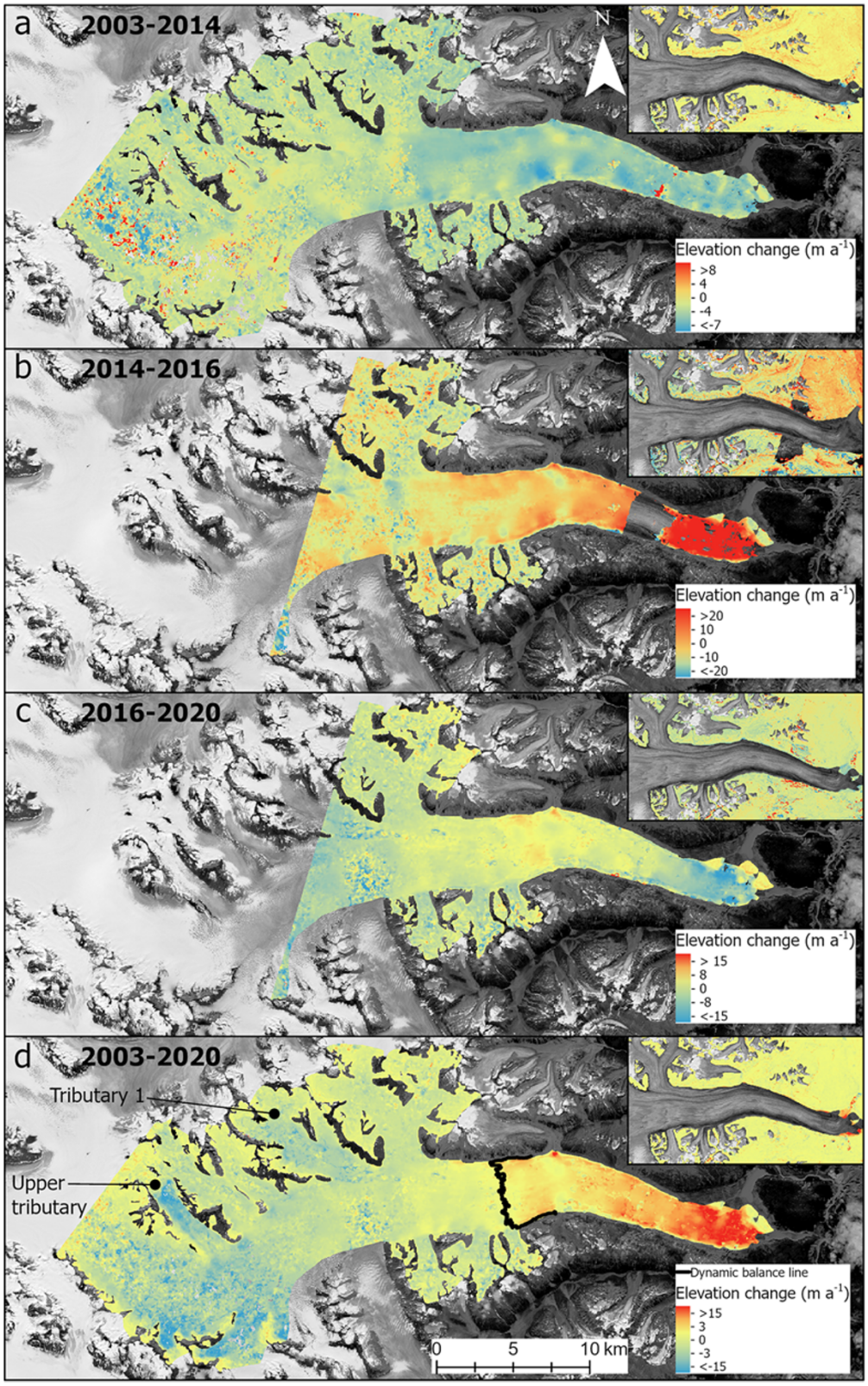

Figure 11. Annual rate of surface elevation change on Fisher Glacier from (a) 2003–14, (b) 2014–16, (c) 2016–20 and (d) entire period 2003–20 (derived from 9 MMASTER DEMs). The dynamic balance line for this period is shown as a black line. Insets in the top right of each panel show the apparent surface elevation change over stable ground for the corresponding period. Base image: Sentinel-2, 12 August 2022.

Our results also give clues as to the possible end date of the historical surge. To start, the point velocities from surface feature-tracking show a mean velocity of 22 m a^{-1} from 1972 to 1976, in line with velocities observed from 2017 onward during the return to quiescence after the recent surge, suggesting that the surge was near its termination in 1972. Second, in the 1976 and 1977 imagery,

the terminus had already begun retreating from its 1972 extent, the crevasses were mainly closed, and small potholes had started to reform. In the recent surge, crevasses took several years to close after velocities reduced and potholes only reappeared in 2021, about 4 years after surge termination, providing further evidence that the 1972 image shows the glacier close to termination. Third, the pattern of elevation changes across Fisher Glacier's surface from 1972 to 1976 (i.e. widespread thinning; green line in Fig. 10a) is similar to the pattern observed from 2016 to 2020 during the most recent switch back to quiescence, which highlights the similarities between both surges and further supports a termination date around 1972.

Based on a combination of historical data and inferences made based on similarities with the recent surge, our reconstruction of the sequence of events surrounding the historical surge is: (i) quiescent phase from at least 1947 to ~1963, (ii) active phase from ~1969 to ~1972, and (iii) quiescence from 1972/73 to 2012. The time between the historical surge's termination and the recent surge's initiation suggests a quiescent phase duration of ~40 years.

5.3. Comparison with other surge-type glaciers in the St. Elias Mountains

Fisher Glacier displays local velocities up to 5.5 m d^{-1} (2000 m a^{-1}) at its peak, although average surge velocities over most of the glacier reached approximately 4 m d^{-1}. These velocities are lower than many surge-type glaciers in the Yukon (Kochtitzky and others, 2019) and fall below the median peak surface velocity of 6.8 m d^{-1} identified by Guillet and others (2025) in the Alaska-Yukon surge cluster. For example, Nàłùdäy (Bevington and Copland, 2014), Variegated (Kamb and others, 1985; Lawson, 1997) and Tweedsmuir (Krimmel and Meier, 1975; Sharp, 2021) glaciers all reached peak velocities of 10 + m d^{-1} during their surges, about double that recorded on Fisher Glacier. Even higher peak velocities have been recorded on Walsh (14 m d^{-1}; Meier and Post, 1969; Fu and Zhou, 2020), Little Kluane (13 m d^{-1}; Main and others, 2024), and Sít' Kusá (Turner; marine-terminating) (up to 25 m d^{-1}; Nolan and others, 2021; Liu and others, 2024) glaciers. However, some large surge-type glaciers in the St. Elias Mountains do display similar speeds to Fisher Glacier, such as Klutlan Glacier which experienced velocities of 4+ m d^{-1} in its 2014–18 surge (Altena and others, 2019; Samsonov and others, 2021), and Dän Zhùr which flows at 2.0–4.5 m d^{-1}, depending on the surge (Abe and others, 2016; Kochtitzky and others, 2019). Conversely, the few small polythermal surge-type glaciers in the St. Elias Mountains display much lower peak surge velocities of 0.12 m d^{-1} (Trapridge Glacier; Frappé and Clarke, 2007) and 0.05–0.10 m d^{-1} (South Glacier; De Paoli and Flowers, 2009).

Fisher Glacier's ~3 year active phase duration is comparable to that of the other glaciers in the St. Elias Mountains. Variegated, Nàłùdäy, Dän Zhùr, Tweedsmuir, Sít' Kusá, and Little Kluane glaciers all have active phases that typically last less than 3 years (Meier and Post, 1969; Krimmel and Meier, 1975; Kamb and others, 1985; Lawson, 1997; Bevington and Copland, 2014; Abe and others, 2016; Kochtitzky and others, 2019; Nolan and others, 2021; Samsonov and others, 2021; Main and others, 2024), whereas Walsh and Klutlan glaciers both exhibit active phases lasting up to 4 years (Fu and Zhou, 2020; Samsonov and others, 2021). Guillet and others (2025) report a median surge duration of 2.3 years in Alaska-Yukon from 2000 to 2024. Fisher Glacier's active phase duration is therefore in the middle- to upper-end of the typical range and is within the range initially described by Meier and Post (1969).

The recent surge of Fisher Glacier initiated in the winter or early spring, similar to Variegated, Walsh, Sít' Kusá, Little Kluane, possibly Klutlan and some of Tweedsmuir's past surges (Kamb and others, 1985; Lawson, 1997; Altena and others, 2019; Nolan and others, 2021; Samsonov and others, 2021; Sharp, 2021; Liu and others, 2024; Main and others, 2024). Conversely, Nàłùdäy's surges typically initiate in late summer or early fall (Bevington and Copland, 2014), while Dän Zhùr is alone with a summer initiation time (Abe and others, 2016; Kochtitzky and others, 2019). Surges in the St. Elias Mountains show a clear pattern of active phase termination during the summer, including for Fisher Glacier.

Fisher Glacier's surges initiate and terminate from the central section of the trunk, and the surge propagates both up- and down-glacier, although the up-glacier progression is a little more subdued (i.e. lower peak velocities than the down-glacier progression). This is uncommon among glaciers in the St. Elias Mountains. Most glaciers have surges that initiate in the mid- to upper-glacier and progress down-glacier from the initiation point. Notably, Walsh, Variegated, Sít' Kusá and Little Kluane glaciers all initiate in their upper region and propagate down-glacier from the initiation location (Lawson, 1997; Samsonov and others, 2021; Liu and others, 2024; Main and others, 2024). Like Fisher Glacier, Klutlan and Dän Zhùr glaciers also initiate in the mid-trunk. However, Dän Zhùr's surges only affect the lower 20 km of the glacier as the surge front only progresses down-glacier from the initiation point at 18–22 km from the terminus (Abe and others, 2016; Kochtitzky and others, 2019). Klutlan Glacier's surges are similar to Fisher Glacier's because it is one of the rare cases where the surge spreads both up- and down-glacier, although its 2014 surge primarily affected the area downstream from the initiation point (Altena and others, 2019; Samsonov and others, 2021) and the up-glacier progression of Klutlan Glacier's surge was limited in extent to its westernmost basin (Altena and others, 2019).

Comparing Fisher Glacier's recent surge to the characteristics of surge-type glaciers in other regions shows that its termination phase is much more rapid and abrupt than most surges in Svalbard-Russian Arctic and High Mountain Asia, and its surge duration is also shorter than the median in these regions (Guillet and others, 2025). That being said, comparing an individual surge event to an entire region can be misleading as there are numerous examples of surges within these regions which share similar characteristics to Fisher's (e.g. Sortebræ's active phase length of ~2.5 years (Pritchard and others, 2005), Monacobreen's peak surface velocities of 4.5 m d^{-1} (Murray and others, 2003; Mansell and others, 2012; Banerjee and others, 2022), and Khurdopin Glacier's surge timing (Quincey and others, 2011; Quincey and Luckman, 2014)).

5.4. Surge mechanisms of Fisher Glacier

Given the characteristics and timing of the two surges described for Fisher Glacier, and those found elsewhere, we can make inferences concerning the likely mechanism(s) that caused them. Some of the main characteristics seen in surges traditionally assigned to a hydrological control are short active phases lasting 1–3 years followed by short quiescent phases of about 10–40 years (Meier and Post, 1969; Kamb and others, 1985; Lawson, 1997), rapid surge initiation in the late autumn or winter (Kamb and others, 1985; Lawson, 1997) and an abrupt surge termination in the late summer (Kamb and others, 1985; Lawson, 1997; Murray and others, 2003; Bevington and Copland, 2014; Abe and others, 2016). Conversely,

surges traditionally assigned to a thermal control typically have longer active phases of 3–10+ years, longer quiescent phases of 50+ years, a gradual surge initiation and/or termination, and the surge initiation and termination timing is variable (i.e. no defined season) (Copland and others, 2003; Murray and others, 2003; Quincey and others, 2011).

During Fisher Glacier's recent surge, the three winters from 2014 to 2016 were the periods with the most activity (greatest velocity changes, most significant terminus advances, appearance of crevasses), which is suggestive of a hydrological control on the surging. Since there is less water reaching the bed in the winter months, any subglacial drainage conduits that were formed during the summer get overpowered by the ice overburden pressure, which collapses them and disperses the water into an inefficient/dispersed subglacial drainage system. This inefficient drainage system is highly pressurized and leads to increased basal sliding and, ultimately, increased velocities (Kamb and others, 1985). Fisher Glacier's rapid termination at the end of the summer also aligns with the hydrologic control mechanism, since increased water input from summer melt can create large drainage conduits, which decrease sliding (Kamb and others, 1985; Benn and others, 2019a). The similar timing of Fisher Glacier's and Sít' Kusá's latest surges may further support the evidence of hydrologically controlled surging at Fisher Glacier. Liu and others (2024) surmise that accumulated mass balance in the reservoir zone exceeding a critical driving stress seems to regulate Sít' Kusá's surge recurrence overall, but that annual meltwater input leading to high basal enthalpy appears to be a driving force in modulating the surge's initiation. Under this proposed mechanism, Fisher Glacier's multidecadal speedup may be the result of a gradual mass balance accumulation in the reservoir zone, while a year with a particularly elevated meltwater input could have triggered the surge.

Although the active phase length and the timing of surge initiation and termination show evidence of a hydrologically controlled surge, Fisher Glacier also displays characteristics that are not typical of hydrologically controlled surges. Notably, its relatively long quiescent phase of ~40 years and the multidecadal pre-surge velocity buildup are uncharacteristic of a hydrologic surge mechanism. It therefore seems that Fisher Glacier's surges may be the result of an interaction between various controls, but further research is needed to elucidate the mechanisms at play, particularly in the central region of the glacier around 22 km up-glacier from the terminus. This region plays a key role in Fisher Glacier's surges as it is the location where the recent surge initiated and terminated, and it is from here that the multidecadal velocity increase originated. This location is also just down-glacier from Tributary 1 (i.e. a main tributary that seems to speed up and contribute to the down-glacier mass transfer during a surge; Fig. 11), and approximately at the location of the DBL from 1954 to 1972. Its surge dynamics may also be better explained by a newer framework such as the enthalpy balance theory (Sevestre and Benn, 2015; Benn and others, 2019a, 2019b, 2022).

5.5. Implications for Fisher Glacier's future surges

Although the two surges broadly resembled each other in terms of general patterns, the maximum terminus extent reached in the ~1972 surge (15.86 ± 0.06 km^2) was greater than in 2016 (7.88 ± 0.04 km^2), and the maximum height of the ice was much higher in the earlier surge. The northern terminus in the historical surge reached a maximum extent only 0.9 km away from the western bank of the Alsek River, whereas the recent surge's maximum extent was ~2.8 km away. Although the historical surge came relatively close to reaching the river in 1972, the likelihood of Fisher Glacier damming it in the future is low because under current and projected future climate conditions all glaciers in this region are expected to maintain a negative mass balance (Berthier and others, 2010; Liu and others, 2022). Accordingly, we expect Fisher Glacier's future surges to reach successively smaller extents, as has happened at Nàłùdäy (Bevington and Copland, 2014) and Dän Zhùr (Kochtitzky and others, 2019). Topographic restrictions have also limited the change in extent of the central and southern parts of the terminus during the past two surges, meaning that the northern section would be the only one with potential for blocking the Alsek River, but this is extremely unlikely under current trends due to the mass balance implications discussed above.

6. Conclusions and future outlook

This study demonstrates that Fisher Glacier has undergone two full surges over the past ~70 years. Its surge history can be broken into 5 distinct periods:

(i) Quiescent phase 1 (1947–68/69): 21+ year long period during which the terminus progressively retreated, and ice thinned in the lower receiving zone and thickened in the upper reservoir zone. The ice surface was characterized by potholes, and there were few crevasses. Assuming similar surge dynamics to its recent history, we suggest that a pre-surge buildup phase would have occurred from ~1964 to 1968/69.

(ii) Active phase 1 (historic surge; ~1969–72): The terminus advanced by several hundred meters and thickened by tens of meters as mass was transferred down-glacier, and the glacier surface became heavily crevassed, particularly along its margins and in the terminus region. Fisher Glacier reached its maximum documented extent of ~0.9 km from the Alsek River during this surge.

(iii) Quiescent phase 2 (1972/73–2012): A 40 year period characterized by low velocities, but which increased gradually (by ~2 m a^{-1}) since at least the mid-1980s, spreading both up- and down-glacier from the central region of the trunk at ~22 km up-glacier from the terminus. The terminus experienced sustained retreat during this time, and the ice surface was generally smooth with only potholes and moulins visible in some areas. The reservoir zone was subject to thickening, and the terminus thinned, both by tens of meters. A pre-surge buildup began around 2008–10, during which velocities in the central region of the glacier increased at an accelerated rate for 3–5 years before reaching active phase velocities of >200 m a^{-1}.

(iv) Active phase 2 (recent surge; 2013–16): The velocities increased significantly (to ~1500 m a^{-1}) in the middle of the glacier and propagated both up- and down-glacier. Although there was no clearly defined initiation time or surge front, the greatest velocity increases and terminus advances occurred each winter during the three surge years. Velocities peaked at >2100 m a^{-1} in winter 2016 at ~12 km from the terminus and dropped rapidly along most of the glacier's length over a period of 1–2 months in late summer 2016. The surge termination occurred first in the middle part of the glacier, near where it initiated, and spread up-glacier and down-glacier from there. During this active phase, the receiving zone thickened by a mean of 32 ± 10 m while the reservoir zone thinned by a mean of 16 ± 10 m, the terminus

advanced by a terminus-wide mean of 868 ± 8 m and crevasses developed across the glacier's surface.

(v) Quiescent phase 3 (ongoing since 2017): By early 2017, velocities returned to quiescent speeds ($<$50 m a^{-1}) along the entire length of the glacier and the regular seasonal velocity pattern (i.e. midsummer speedup) returned. Additionally, the crevasses and seracs closed up and potholes started developing ~4 years after surge termination.

The timing of Fisher Glacier's peak surge velocity in winter, and summer termination, align with what is traditionally attributed to a hydrological surge control, as does the abrupt termination and the short active phase length. However, its multidecadal velocity increase prior to the most recent surge aligns with what is traditionally attributed to a thermal control. An unusual attribute is the double surge front which progresses both up- and down-glacier from the initiation point in the middle of the glacier. Thus, the observed surge dynamics support the increasingly popular notion of dynamically unifying processes driving glacier surges, rather than a singular process, meaning that the enthalpy balance theory may provide a better framework with which to understand the cause of Fisher Glacier's surges (Sevestre and Benn, 2015; Benn and others, 2019a, 2019b, 2022).

This study provides a reconstruction of Fisher Glacier's previous surges and a base from which we can carry out more detailed studies that focus on particular aspects of its surge dynamics. It is highly likely that future surges of Fisher Glacier will not dam the Alsek River, although water inputs from the glacier could contribute to changing river water levels. Future work that could improve understanding of the mechanisms at play and the physical properties of the glacier that contribute to surging include ice penetrating radar to determine the glacier's thickness and basal topography, and measurements of englacial and basal ice temperatures.

Supplementary material. The supplementary material for this article can be found at https://doi.org/10.1017/jog.2025.10084.

Acknowledgements. Support for this research has been provided by the University of Ottawa, Northern Scientific Training Program, Remote-Ex Norwegian/Canadian/American Partnership Program, Natural Sciences and Engineering Research Council of Canada (NSERC) Discovery Grant and Northern Supplement, NSERC Canada Graduate Scholarship – Master's, Polar Continental Shelf Program, ArcticNet Network of Centres of Excellence Canada, Canada Foundation for Innovation, Ontario Research Fund and Kluane Lake Research Station. We thank Champagne and Aishihik First Nations and Parks Canada, who provided the permissions required for our fieldwork. We also acknowledge two anonymous reviewers, Scientific Editor Rakesh Bhambri and Associate Chief Editor Hester Jiskoot for useful comments which helped improve the manuscript.

Competing interests. The authors declare that they have no competing interests for this paper.

References

Abe T, Furuya M and Sakakibara D (2016) Brief Communication: Twelve-year cyclic surging episodes at Donjek Glacier in Yukon, Canada. *The Cryosphere* **10**, 1427–1432. doi:10.5194/tc-10-1427-2016

Altena B, Scambos T, Fahnestock M and Kääb A (2019) Extracting recent short-term glacier velocity evolution over southern Alaska and the Yukon from a large collection of Landsat data. *The Cryosphere* **13**(3), 795–814. doi:10.5194/tc-13-795-2019

Banerjee D, Garg V and Thakur PK (2022) Geospatial investigation on transitional (quiescence to surge initiation) phase dynamics of Monacobreen tidewater glacier, Svalbard. *Advances in Space Research* **69**(4), 1813–1839. doi:10.1016/j.asr.2021.08.020

Benn DI, Fowler AC, Hewitt I and Sevestre H (2019a) A general theory of glacier surges. *Journal of Glaciology* **65**(253), 701–716. doi:10.1017/jog.2019.62

Benn DI, Hewitt IJ and Luckman AJ (2022) Enthalpy balance theory unifies diverse glacier surge behaviour. *Annals of Glaciology* **63**(87-89), 88–94. doi:10.1017/aog.2023.23

Benn DI, Jones RL, Luckman A, Fürst JJ, Hewitt I and Sommer C (2019b) Mass and enthalpy budget evolution during the surge of a polythermal glacier: A test of theory. *Journal of Glaciology* **65**(253), 717–731. doi:10.1017/jog.2019.63

Berthier E, Schiefer E, Clarke GKC, Menounos B and Rémy F (2010) Contribution of Alaskan glaciers to sea level rise derived from satellite imagery. *Nature Geoscience* **3**(2), 92–95. doi:10.1038/ngeo737

Bevington A and Copland L (2014) Characteristics of the last five surges of Lowell Glacier, Yukon, Canada, since 1948. *Journal of Glaciology* **60**(219), 113–123. doi:10.3189/2014JoG13J134

Burgess EW, Forster RR and Larsen CF (2013) Flow velocities of Alaskan glaciers. *Nature Communications* **4**(1), 2146. doi:10.1038/ncomms3146

Ciracì E, Velicogna I and Swenson S (2020) Continuity of the mass loss of the world's glaciers and ice caps from the GRACE and GRACE Follow-On missions. *Geophysical Research Letters* **47**(9), e2019GL086926. doi:10.1029/2019GL086926

Clarke GKC and Holdsworth G (2002) Glaciers of the St Elias Mountains. In Williams RS, Jr. and Ferrigno JG (eds), *Satellite Image Atlas of Glaciers of the World: Glaciers of North America–Glaciers of Canada*. United States Geological Survey, pp. J301–J328. https://pubs.usgs.gov/pp/p1386j/

Clarke GKC, Schmok JP, Ommanney CSL and Collins SG (1986) Characteristics of surge-type glaciers. *Journal of Geophysical Research: Solid Earth* **91**(B7), 7165–7180. doi:10.1029/JB091iB07p07165

Colgan W, Rajaram H, Abdalati W, McCutchan C, Mottram R, Moussavi MS and Grigsby S (2016) Glacier crevasses: Observations, models, and mass balance implications. *Reviews of Geophysics* **54**, 119–161. doi:10.1002/2015RG000504

Copland L, Sharp MJ, and Dowdeswell JA (2003) The distribution and flow characteristics of surge-type glaciers in the Canadian High Arctic. *Annals of Glaciology* **36**, 73–81. doi:10.3189/172756403781816301

De Paoli L and Flowers G (2009) Dynamics of a small surge-type glacier using one-dimensional geophysical inversion. *Journal of Glaciology* **55**(194), 1101–1112. doi:10.3189/002214309790794850

Dolgoushin LD and Osipova GB (1975) Glacier surges and the problem of their forecasting. *IAHS-AISH Publication* **104**, 292–304.

Eisen O, Harrison WD and Raymond CF (2001) The surges of Variegated Glacier, Alaska, USA, and their connection to climate and mass balance. *Journal of Glaciology* **47**(158), 351–358. doi:10.3189/172756501781832179

Eisen O, Harrison WD, Raymond CF, Echelmeyer KA, Bender GA and Gorda JLD (2005) Variegated Glacier, Alaska, USA: A century of surges. *Journal of Glaciology* **51**(174), 399–406. doi:10.3189/172756505781829250

Frappé T-P, and Clarke GKC (2007) Slow surge of Trapridge Glacier, Yukon Territory, Canada. *Journal of Geophysical Research* **112**(F3), F03S32. doi:10.1029/2006JF000607

Fu X and Zhou J (2020) Recent surge behavior of Walsh Glacier revealed by remote sensing data. *Sensors* **20**(3), 716. doi:10.3390/s20030716

Gardner AS, Fahnestock MA and Scambos TA (2019) *ITS_LIVE Regional Glacier and Ice Sheet Surface Velocities*. Data archived at National Snow and Ice Data Center.

Gardner AS, Moholdt G, Scambos T, Fahnstock M, Ligtenberg S, van den Broeke M and Nilsson J (2018) Increased West Antarctic and unchanged East Antarctic ice discharge over the last 7 years. *Cryosphere* **12**(2), 521–547. doi:10.5194/tc-12-521-2018

Girod L, Nuth C, Kääb A, McNabb R and Galland O (2017) MMASTER: Improved ASTER DEMs for elevation change monitoring. *Remote Sensing* **9**(7), 704. doi:10.3390/rs9070704

Guillet G, Benn DI, King O, Shean D, Schytt Mannerfelt E and Hugonnet R (2025) Global detection of glacier surges from surface velocities, elevation

change and SAR backscatter data between 2000 and 2024: A test of surge mechanism theories. *Journal of Glaciology* **71**, e88. doi:10.1017/jog.2025.10065

Hall DK, Bayr KJ, Schöner W, Bindschadler RA and Chien JYL (2003) Consideration of the errors inherent in mapping historical glacier positions in Austria from the ground and space (1893–2001). *Remote Sensing of Environment* **86**, 566–577. doi:10.1016/S0034-4257(03)00134-2

Hambrey M and Alean J (2004) Ice on the move. In *Glaciers*. Cambridge: Cambridge University Press, pp. 69–100. doi:10.1017/CBO9780511807602.006

Herreid S and Truffer M (2016) Automated detection of unstable glacier flow and a spectrum of speedup behavior in the Alaska Range. *Journal of Geophysical Research: Earth Surface* **121**(1), 64–81. doi:10.1002/2015JF003502

Jiskoot H, Murray T and Boyle P (2000) Controls on the distribution of surge-type glaciers in Svalbard. *Journal of Glaciology* **46**(154), 412–422. doi:10.3189/172756500781833115

Kamb B, Raymond CF, Harrison WD, Engelhardt H, Echelmeyer KA, Humphrey N, Brugman MM and Pfeffer T (1985) Glacier surge mechanism: 1982-1983 surge of Variegated Glacier, Alaska. *Science* **227**(4686), 469–479. doi:10.1126/science.227.4686.469

Kochtitzky W, Jiskoot H, Copland L, Enderlin E, McNabb R, Kreutz K and Main B (2019) Terminus advance, kinematics and mass redistribution during eight surges of Donjek Glacier, St. Elias Range, Canada, 1935 to 2016. *Journal of Glaciology* **65**(252), 565–579. doi:10.1017/jog.2019.34

Krimmel RM and Meier MF (1975) Glacier applications of ERTS Images. *Journal of Glaciology* **15**(73), 391–402. doi:10.3189/S002214300003450X

Krumwiede BS, Kamp U, Leonard GJ, Kargel JS, Dashtseren A and Walther M (2014) Recent glacier changes in the Mongolian Al-tai Mountains: Case studies from Munkh Khairkhan and Tavan Bogd. In Kargel J, Leonard G, Bishop M and Kääb A (eds), *Global Land Ice Measurements from Space*. Berlin: Springer, pp. 481–508.

Lauzon B, Copland L, Van Wychen W, Kochtitzky, W, McNabb R, and Dahl-Jensen D (2023) Dynamics throughout a complete surge of Iceberg Glacier on western Axel Heiberg Island, Canadian High Arctic. *Journal of Glaciology* **69**(277), 1333–1350. doi: 10.1017/jog.2023.20

Lawson W (1997) Spatial, temporal and kinematic characteristics of surges of Variegated Glacier, Alaska. *Annals of Glaciology* **24**, 95–101. doi:10.3189/S026030550001199X

Liestøl O, Repp K and Wold B (1980) Supra-glacial lakes in Spitsbergen. *Norsk Geografisk Tiddskrift* **34**(2), 89–92. doi:10.1080/00291958008621919

Liu B, Zou X, Yi S, Sneeuw N, Li J and Cai J (2022) Reconstructing GRACE-like time series of high mountain glacier mass anomalies. *Remote Sensing of Environment* **280**, 113177. doi:10.1016/j.rse.2022.113177

Liu J, Enderlin EM, Bartholomaus TC, Terleth Y, Mikesell TD and Beaud F (2024) Propagating speedups during quiescence escalate to the 2020–2021 surge of Sít' Kusá, southeast Alaska. *Journal of Glaciology* **70**(e57), 1–12. doi:10.1017/jog.2023.99

Main B, Copland L, Flowers G, Dow C, Van Wychen W, Samsonov S and Kochtitzky W (2024) Topographic and hydrological controls on partial and full surges of Little Kluane Glacier, Yukon. *Journal of Glaciology* 1–14. doi:10.1017/jog.2024.35

Mansell D, Luckman A and Murray T (2012) Dynamics of tidewater surge-type glaciers in northwest Svalbard. *Journal of Glaciology* **58**(207), 110–118. doi:10.3189/2012JoG11J058

Medrzycka D, Copland L and Noël B (2023) Rapid demise and committed loss of Bowman Glacier, northern Ellesmere Island, Arctic Canada. *Journal of Glaciology* **69**(276), 997–1010. doi:10.1017/jog.2022.119

Meier MF and Post A (1969) What are glacier surges? *Canadian Journal of Earth Sciences* **6**(4), 807–817. doi:10.1139/e69-081

Murray T, Strozzi T, Luckman A, Jiskoot H, and Christakos P (2003) Is there a single surge mechanism? Contrasts in dynamics between glacier surges in Svalbard and other regions. *Journal of Geophysical Research: Solid Earth* **108**(B5), 2237. doi:10.1029/2002JB001906

Nolan A, Kochtitzky W, Enderlin E, McNabb R and Kreutz K (2021) Kinematics of the exceptionally-short surge cycles of Sít' Kusá (Turner Glacier), Alaska, from 1983 to 2013. *Journal of Glaciology* **67**(264), 744–758. doi:10.1017/jog.2021.29

Nuth C and Kääb A (2011) Co-registration and bias corrections of satellite elevation data sets for quantifying glacier thickness change. *The Cryosphere* **5**(1), 271–290. doi:10.5194/tc-5-271-2011

Porter C, Morin P, Howat I, Noh M-J, Bates B, Peterman K, Keesey S, Schlenk M, Gardiner J and Tomko K and 19 others (2018) ArcticDEM, Version 3. Harvard Dataverse V1. doi:10.7910/DVN/OHH

Pritchard H, Murray T, Luckman A, Strozzi T and Barr S (2005) Glacier surge dynamics of Sortebræ, east Greenland, from synthetic aperture radar feature tracking. *Journal of Geophysical Research* **110**(F3), F03005–n/a. doi:10.1029/2004JF000233

Quincey DJ, Braun M, Glasser NF, Bishop MP, Hewitt K and Luckman A (2011) Karakoram glacier surge dynamics. *Geophysical Research Letters* **38**, L18504. doi:10.1029/2011GL049004

Quincey DJ and Luckman A (2014) Brief Communication: On the magnitude and frequency of Khurdopin glacier surge events. *The Cryosphere* **8**(2), 571–574. doi:10.5194/tc-8-571-2014

RGI Consortium (2017) Randolph Glacier Inventory - A Dataset of Global Glacier Outlines, Version 6.0. Region 1: Alaska. Boulder, Colorado USA. NSIDC: National Snow and Ice Data Center. doi:10.7265/4m1f-gd79

RGI Consortium (2023) Randolph Glacier Inventory - A Dataset of Global Glacier Outlines, Version 7.0. Boulder, Colorado USA. NSIDC: National Snow and Ice Data Center.

Samsonov S, Tiampo K and Cassotto R (2021) Measuring the state and temporal evolution of glaciers in Alaska and Yukon using synthetic-aperture-radar-derived (SAR-derived) 3D time series of glacier surface flow. *The Cryosphere* **15**(9), 4221–4239. doi:10.5194/tc-15-4221-2021

Sevestre H and Benn DI (2015) Climatic and geometric controls on the global distribution of surge-type glaciers: Implications for a unifying model of surging. *Journal of Glaciology* **61**(228), 646–662. doi:10.3189/2015JoG14J136

Sevestre H, Benn DI, Hulton NRJ and Bælum K (2015) Thermal structure of Svalbard glaciers and implications for thermal switch models of glacier surging. *Journal of Geophysical Research Earth Surface* **120**(10), 2220–2236. doi:10.1002/2015JF003517

Sharp M (2021) *Amplification of Surface Topography During Surges of Tweedsmuir Glacier*, MSc thesis, University of Calgary. doi: 10.11575/PRISM/39300

Sturm M (1987) Observations on the distribution and characteristics of potholes on surging glaciers. *Journal of Geophysical Research* **92**(B9), 9015–9022. doi:10.1029/JB092iB09p09015

Sund M, Eiken T, Hagen JO and Kääb A (2009) Svalbard surge dynamics derived from geometric changes. *Annals of Glaciology* **50**(52), 50–60. doi:10.3189/172756409789624265

Urbanski JA (2018) A GIS tool for two-dimensional glacier-terminus change tracking. *Computers & Geosciences* **111**, 97–104. doi:10.1016/j.cageo.2017.11.004

Van Wychen W, Copland L, Jiskoot H, Gray L, Sharp M and Burgess D (2018) Surface velocities of glaciers in western Canada from speckle-tracking of ALOS PALSAR and RADARSAT-2 data. *Canadian Journal of Remote Sensing* **44**(1), 57–66. doi:10.1080/07038992.2018.1433529

Williamson SN and 9 others (2020) Evidence for elevation-dependent warming in the St. Elias Mountains, Yukon, Canada. *Journal of Climate* **33**, 3253–3269. doi:10.1175/JCLI-D-19-0405.1

Young EM, Flowers GE, Jiskoot H and Gibson HD (2024) Reconstructing glacier surge kinematics using a numerical ice-flow model applied to the Dusty Glacier, St. Elias Mountains, Canada. *Geophysical Research Letters* **51**, e2023GL107386. doi:10.1029/2023GL107386